Cluster-expansion representation in quantum optics

M. Kira and S. W. Koch
Department of Physics and Material Sciences Center, Philipps-University Marburg, Renthof 5, D-35032 Marburg, Germany
(Received 20 March 2008; published 11 August 2008)

A theoretical framework is developed that combines the systematic many-body cluster-expansion approach with the standard quantum-optical representations. A cluster-expansion transformation is derived to obtain a flexible one-to-one mapping between correlated clusters and the usual phase-space and marginal distributions discussed in quantum optics. The convergence and correlation properties of this transformation are explored through several quantum-field examples including coherent, thermal, squeezed, Fock, and Schrödinger cat states. The resulting correlation properties can be used as a basis to characterize and control many-body correlations when quantum light interacts with matter. As an application, a cluster-expansion-restoration scheme is developed that allows for the retrieval of the true quantum statistics of light from realistic measurements that are deteriorated by the reduced quantum efficiency of the detectors.

DOI: 10.1103/PhysRevA.78.022102 PACS number(s): 03.65.Wj, 42.50.Dv, 42.50.Lc

I. INTRODUCTION

Quantum-optical investigations can often be reduced to the analysis of a model system where one isolates a few light modes that interact with a simple quantized material such as a two-level atom [1–3]. This approach yields the well-known Jaynes-Cummings model [4] and its straightforward extensions including multiple atoms [5] and light modes [6]. Furthermore, one can introduce the coupling to one or more reservoirs [7–9] introducing decay processes. With the help of these models, one can explain a wide variety of phenomena ranging from reversible spontaneous emission [10,11] and quantum-Rabi flopping [12] to intriguing entanglement effects and their applications [13–20]. For the rigorous analysis of these effects, one needs to know the quantum statistics, i.e., the fundamental distribution function characterizing all quantum fluctuation aspects of the studied light. Practically, the quantum statistics can be described via the density matrix (or wave function if it exists), the Wigner function, or many alternative equivalent forms. In general, the quantum-statistical analysis of single-mode light fields is well established [21–23]. Especially, there are several criteria for nonclassical behavior such as squeezing below the Heisenberg minimum-uncertainty limit [24], antibunching [25,26], emergence of negative values in the Wigner function [27], or the violation of Bell's inequalities [28].

The standard quantum-statistical analysis of light-matter interaction often becomes impractical in situations where a few-level description of the matter part of the system is no longer adequate and a genuine many-body approach has to be used. It is difficult—if not impossible—to use wave functions, density matrices, or the Wigner function simply because the dimension of these objects becomes unmanageably large, as far as current numerical resources are concerned. Hence, one has to resort to an alternative approach where one determines the quantum statistics via expectation values and eventually via different levels of correlations. For example, one can apply the so-called cluster-expansion scheme to systematically include correlations up to a desired level. Since the dimension of the included clusters is typically much smaller than that of the system, this scheme allows for a computationally feasible description of the coupled light-matter quantum statistics. The cluster-expansion approach has already been applied [29] in systematic treatments of the combined quantum-optical and semiconductor many-body correlations yielding, e.g., a microscopic description of photoluminescence [30,31], squeezing [32], and entanglement effects [33–35]. On this basis, we introduced the quantum-optical spectroscopy [36] in semiconductors where the quantum statistics of light is utilized, e.g., to directly create desired many-body states with modified interaction properties.

In this paper, we analyze how the cluster-expansion approach is connected to well-established quantum-optical concepts for single-mode systems by developing the cluster-expansion-based representation for the quantum statistics of light. In particular, we extend the cumulant-expansion approaches [37] beyond the diagonal occupation of number states. Besides verifying that our approach can be reduced to known quantum-statistical representations, we show that it also provides a simple description of many relevant quantum fields. In addition, we demonstrate that the cluster-expansion method can be applied to remove quantum-efficiency deterioration effects that are often present in realistic quantum-statistics measurements, allowing us to restore the true quantum-statistical information from actual measurements.

This paper is organized as follows. We first discuss in Sec. II how the cluster expansion provides a systematic scheme for both the many-body and quantum-optical problems. The formalism is then applied for a single-mode light field in Sec. III. In Sec. IV, the results are then developed into an operational cluster expansion for a single-mode light with a generic quantum statistics. The derived cluster-expansion transformation (CET) is analyzed thoroughly in Sec. V, where the convergence criteria are derived and tested via several numerical examples. Finally in Sec. VI, we formulate the cluster-expansion restoration (CER) transformation that can be applied directly to experimental data to restore the true quantum statistics from corrupted measurements.

II. QUANTUM OPTICS AND CLUSTER EXPANSION

The quantization of the transversal electromagnetic field can be performed in several equivalent ways. Here, we resort

to the mode-expansion formulation where the first step is to find the complete set of orthogonal and transversal mode functions $\mathbf{u}_\mathbf{q}(\mathbf{r})$ that are steady-state solutions of the wave equation, i.e., $\mathbf{u}_\mathbf{q}(\mathbf{r})$ fulfills the Helmholtz equation without the optically active matter. In free space, the mode functions are plane waves, $\mathbf{u}_\mathbf{q}(\mathbf{r})=\frac{1}{\sqrt{\mathcal{V}}}e^{\mathbf{q}\cdot\mathbf{r}}\mathbf{e}_\mathbf{q}$, where $\mathcal{V}$ is the quantization volume, $\mathbf{q}$ is the wave vector, and $\mathbf{e}_\mathbf{q}$ is the unit vector of the polarization direction. The quantized light field is expressed as [38,39]

$$\mathbf{E}(\mathbf{r})=\sum_\mathbf{q}[i\mathcal{E}_\mathbf{q}\mathbf{u}_\mathbf{q}(\mathbf{r})\hat{B}_\mathbf{q}+\text{H.c.}], \tag{1}$$

where the mode index $\mathbf{q}$ also contains the polarization direction. The actual quantization of the multimode field follows after one demands [38] that each coefficient obey the bosonic commutation rules $[\hat{B}_\mathbf{q},\hat{B}^\dagger_{\mathbf{q}'}]_-=\hat{B}_\mathbf{q}\hat{B}^\dagger_{\mathbf{q}'}-\hat{B}^\dagger_{\mathbf{q}'}\hat{B}_\mathbf{q}=\delta_{\mathbf{q},\mathbf{q}'}$ and $[\hat{B}_\mathbf{q},\hat{B}_\mathbf{q}]_-=[\hat{B}^\dagger_\mathbf{q},\hat{B}^\dagger_{\mathbf{q}'}]_-=0$. The quantization procedure also fixes the vacuum-field amplitude, $\mathcal{E}_\mathbf{q}=\sqrt{\hbar\omega_\mathbf{q}/(2\epsilon_0)}$, where $\omega_\mathbf{q}=c|\mathbf{q}|$ is the frequency of the mode, ϵ_0 is the permittivity of the vacuum, and c is the speed of light in free space.

A. Hierarchy problem arising from light-matter coupling

The coupling of matter to the multimode light field can be formulated with the help of the dipole-interaction Hamiltonian,

$$\hat{H}_\text{sys}=\sum_\mathbf{q}\hbar\omega_\mathbf{q}\left(\hat{B}^\dagger_\mathbf{q}\hat{B}_\mathbf{q}+\frac{1}{2}\right)-\sum_\mathbf{q}(g^\star_\mathbf{q}\hat{B}^\dagger_\mathbf{q}\hat{P}_\mathbf{q}+g_\mathbf{q}\hat{B}_\mathbf{q}\hat{P}^\dagger_\mathbf{q})+\hat{H}_\text{mat}, \tag{2}$$

where $g_\mathbf{q}$ determines the coupling strength of light to the matter polarization $\hat{P}_\mathbf{q}$ while the pure mater contributions are implicitly given by $\hat{H}_\text{mat}$; for the explicit forms, we refer to Ref. [40]. The Hamiltonian (2) can be reduced to the familiar Jaynes-Cummings form by restricting the analysis to the single mode $\hat{B}\equiv\hat{B}_\mathbf{q}$ and identifying the polarization $\hat{P}_\mathbf{q}\equiv\sigma_-$ via the usual lowering operator for the two-level system. In the same way, the semiconductor form is found by introducing the polarization operator $\hat{P}_\mathbf{q}=\Sigma_{\mathbf{k},\lambda\neq\lambda'}\hat{a}^\dagger_{\lambda,\mathbf{k}}\hat{a}_{\lambda',\mathbf{k}+\mathbf{q}}$, which describes electronic interband coherences. Since the electrons are fermions, they obey the usual anticommutation relations $[\hat{a}^\dagger_{\lambda,\mathbf{k}}\hat{a}_{\lambda',\mathbf{k}'}]_+=\delta_{\lambda,\lambda'}\delta_{\mathbf{k},\mathbf{k}'}$. The resulting light-matter interaction conserves the total momentum since the photon momentum is always balanced by the corresponding recoil momentum in the carrier system. In low-dimensional semiconductors, the momentum conservation is only partial since only some of its components—corresponding to the unconfined space dimensions—are conserved. One can easily generalize the light-matter interaction also for cases in which the coupling strength depends on both band and momentum indices.

Since the density-matrix- or wave-function-based solutions are impractical for multimode fields and/or semiconductor investigations, we adopt an equation-of-motion approach that can be generally applied. Hence, we evaluate the Heisenberg equation of motion for the relevant operators,

$$i\hbar\frac{\partial}{\partial t}\hat{O}=[\hat{O},\hat{H}_\text{sys}]_-,\quad\langle\hat{O}\rangle\equiv\text{Tr}[\hat{O}\hat{\rho}], \tag{3}$$

and compute the observables using the density matrix $\hat{\rho}$. The time evolution for the light is then obtained from the photon-operator dynamics,

$$i\hbar\frac{\partial}{\partial t}\hat{B}_\mathbf{q}=\hbar\omega_\mathbf{q}\hat{B}_\mathbf{q}-g^\star_\mathbf{q}\hat{P}_\mathbf{q},$$

$$i\hbar\frac{\partial}{\partial t}\hat{B}^\dagger_\mathbf{q}=-\hbar\omega_\mathbf{q}\hat{B}^\dagger_\mathbf{q}+g_\mathbf{q}P^\dagger_\mathbf{q}. \tag{4}$$

To complete these equations, we also need the polarization-operator dynamics,

$$i\hbar\frac{\partial}{\partial t}\hat{P}_\mathbf{q}=-\sum_{\mathbf{q}'}(g^\star_{\mathbf{q}'}\hat{B}^\dagger_\mathbf{q}[\hat{P}_\mathbf{q},\hat{P}_{\mathbf{q}'}]_-+g_{\mathbf{q}'}\hat{B}_\mathbf{q}[\hat{P}_\mathbf{q},\hat{P}^\dagger_{\mathbf{q}'}]_-)$$
$$+[\hat{P}_\mathbf{q},H_\text{mat}]_-. \tag{5}$$

The polarization dynamics due to light-matter coupling yields a simple closed form as long as the polarizaton operators obey fully bosonic commutation relations, i.e., $[\hat{P}_\mathbf{q},\hat{P}_{\mathbf{q}'}]_-=0$ and $[\hat{P}_\mathbf{q},\hat{P}^\dagger_{\mathbf{q}'}]_-=\delta_{\mathbf{q},\mathbf{q}'}$. In this bosonic scenario, the light-matter coupling Hamiltonian leads to a direct transfer of the light quantum statistics to the matter system. This transfer also works reasonably well even when $\hat{P}_\mathbf{q}$ is weakly nonbosonic. For example, we have shown [36] that the light quantum statistics can be transferred to a sufficiently dilute exciton system where scattering and phase-space effects are only of minor importance.

For systems in which the polarization operators are nonbosonic, such as $\sigma_\pm$ or the interband polarization in semiconductors, one actually has to include the nontrivial forms of $[\hat{P}_\mathbf{q},\hat{P}_{\mathbf{q}'}]_-$ and $[\hat{P}_\mathbf{q},\hat{P}^\dagger_{\mathbf{q}'}]_-$ in the analysis. In general, when working out the equations of motions, these commutations lead to the appearance of new operator combinations, other than polarization. Thus, one actually needs to solve the equation of motion for these new objects. Since new operator combinations emerge for each new equation, one ends up with an infinite hierarchy of operator equations. It is notable that this hierarchy problem already arises from the quantum-optical light-matter coupling, which can be verified even for the simplest Jaynes-Cummings-model analysis. Besides this quantum-optical hierarchy problem, semiconductor investigations involve additional hierarchical couplings, e.g., due to the Coulomb many-body interaction resulting from the $[\hat{P}_\mathbf{q},H_\text{mat}]_-$ contribution.

B. Cluster-expansion solution

A systematic way to treat the quantum-mechanical hierarchy problem is provided by the cluster-expansion method [29,41–46]. This approach is well established, e.g., in quantum chemistry, where it has been applied to solve the many-body eigenstates of molecules [43–45]. In semiconductor

systems, this formalism has successfully been used to explain a variety of many-body and quantum-optical phenomena [32,36,39,46–55]. In the following, we briefly summarize the main aspects of the cluster-expansion scheme based on the discussion in Ref. [29].

From a purely formal point of view, both a photon and a polarization operator constitute a single-particle operator. If we use the semiconductor as an example, a general N-particle operator has the form

$$\hat{N} = \hat{B}_1^\dagger \cdots \hat{B}_{N_1}^\dagger \hat{a}_1^\dagger \cdots \hat{a}_{N_2}^\dagger \hat{a}_{N_2} \cdots \hat{a}_1 \hat{B}_{N_3} \cdots \hat{B}_1 \tag{6}$$

with all possible combinations of N_j fulfilling $N_1+N_2+N_3=N$. We have used here a compact notation where the j in $\hat{B}_j$ is a generic photon index $\mathbf{q}_j$. Based on the identification (6), we notice that the light-matter interaction in Eq. (2) constitutes a genuine two-particle interaction for systems with a nonbosonic polarization. Thus, it is not surprising that we end up with formally identical hierarchy problems, connecting N- and $(N+1)$-particle expectation values via

$$i\hbar \frac{\partial}{\partial t} \langle \hat{N} \rangle = F_{\text{free}}[\langle \hat{N} \rangle] + F_{\text{hier}}[\langle \hat{N}+1 \rangle] \tag{7}$$

for both the light-matter and the electronic two-particle Coulomb interactions. In Eq. (7), the functional F_{free} results from the noninteracting part while F_{hier} originates from the two-particle interactions.

Identifying the dominant contributions for many-body and quantum-optical systems, one can often identify a finite number of correlated clusters that correspond to the low-rank momenta of simple distributions. In these cases, one can describe the quantum statistics with quantities whose number is significantly reduced relative to the original, often infinite-dimensional, distribution. For example, when the many-body and the quantum-optical properties are accurately described by the C lowest clusters, the hierarchy problem can be systematically truncated based on the cluster order appearing in Eq. (7).

To operationalize the cluster-expansion truncation, we have to determine all the consistent factorizations of an N-particle quantity $\langle \hat{N} \rangle$ in terms of (i) independent single particles (singlets), (ii) correlated pairs (doublets), (iii) correlated three-particle clusters (triplets), up to (iv) correlated N-particle clusters. For example, the pure photon terms have a simple singlet factorization

$$\langle \hat{B}_1^\dagger \cdots \hat{B}_M^\dagger \hat{B}_{M+1} \cdots \hat{B}_1 \rangle_S = \langle \hat{B}_1^\dagger \rangle \cdots \langle \hat{B}_M^\dagger \rangle \langle \hat{B}_{M+1} \rangle \cdots \langle \hat{B}_1 \rangle, \tag{8}$$

which is identical to the classical factorization since each bosonic operator is simply replaced by a complex-valued quantity. At the next level, the system may display pairwise correlations in the form of doublets,

$$\Delta\langle \hat{B}_1^\dagger \hat{B}_{1'} \rangle \equiv \langle \hat{B}_1^\dagger \hat{B}_{1'} \rangle - \langle \hat{B}_1^\dagger \hat{B}_{1'} \rangle_S,$$

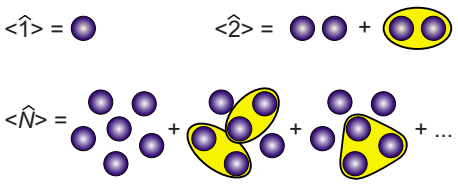

FIG. 1. (Color online) Schematic factorization of bosonic N-particle expectation values into correlated clusters.

$$\Delta\langle \hat{B}_1 \hat{B}_{1'} \rangle \equiv \langle \hat{B}_1 \hat{B}_{1'} \rangle - \langle \hat{B}_1 \hat{B}_{1'} \rangle_S. \tag{9}$$

These contributions already describe the onset of quantum-optical correlations. The expansion can be continued up to the desired level of correlated N-particle clusters if we formally know all expectation values from $\langle \hat{1} \rangle$ to $\langle \hat{N} \rangle$. Then, a specific correlated cluster can be constructed recursively using

$$\langle \hat{3} \rangle = \langle \hat{3} \rangle_S + \langle \hat{1} \rangle \Delta\langle \hat{2} \rangle + \Delta\langle \hat{3} \rangle,$$

$$\langle \hat{N} \rangle = \langle \hat{N} \rangle_S + \langle \hat{N}-1 \rangle_S \Delta\langle \hat{2} \rangle + \langle \hat{N}-4 \rangle_S \Delta\langle \hat{2} \rangle \Delta\langle \hat{2} \rangle + \cdots + \langle \hat{N}-3 \rangle_S \Delta\langle \hat{3} \rangle + \cdots + \Delta\langle \hat{N} \rangle. \tag{10}$$

Here, the quantities with the subscript S denote the singlet contributions and the terms $\Delta\langle \hat{J} \rangle$ contain the purely correlated parts of the J-particle cluster. In Eq. (10), each term includes a sum over all *unique* possibilities to reorganize the N indices among singlets, doublets, and so on. Thus, one must sum over all *indistinguishable* permutations of operator indices such that each combination is included once and only once. The fundamental fermionic and/or bosonic indistinguishability is guaranteed by associating the appropriate sign with the permutations: for bosons, all permutations have a positive sign while odd (even) permutations have a negative (positive) sign for fermions. The schematic representation of Eqs. (8)–(10) is shown in Fig. 1.

Even though we can associate a certain number of photon operators with N-particle quantities, the photons should not literally be taken as particles. In the cluster-expansion approach, the particle concept—strictly speaking—refers to a given class of expectation values or correlations. Nonetheless, the formal particle concept actually allows us to *systematically isolate* the physically and intuitively important aspects from the full quantum statistics. In particular, the cluster factorizations represent all possible ways "particles" can be correlated with each other when the level of correlation is limited to C. This observation allows us to apply the systematic cluster-expansion truncation that is obtained by decomposing any given N-particle quantity into C-particle correlations,

$$\langle \hat{N} \rangle_{1\cdots C} \equiv \langle \hat{N} \rangle_S + \langle \hat{N} \rangle_D + \cdots + \langle \hat{N} \rangle_C = \sum_{J=1}^{C} \langle \hat{N} \rangle_J, \tag{11}$$

following directly from Eq. (10). Here, $\langle N \rangle_S$ contains only singlets, $\langle N \rangle_D$ contains all combinations of doublets but no higher-order correlations, and so on. This truncation is physi-

cally meaningful since one often excites the system with weakly correlated light such as that emitted from most lasers. In this situation, the higher-order correlations build up in a strictly hierarchical order from $\Delta\langle\hat{J}\rangle$ to $\Delta\langle\hat{J}+1\rangle$ via the two-particle interactions. Thus, as long as we start from an uncorrelated, Hartree-Fock-like ground state, we always find a physically relevant time window where only clusters below C-particle correlations determine the essential system properties. The nature of the physical problem determines the lowest meaningful value of C. For example, if photons have only pairwise correlations, the light can become squeezed. The description of this process does not require clusters beyond $C=2$.

For any given light source, one can always limit the photon correlations to a phase space where correlated clusters beyond C are less important. Thus, the hierarchy problem (7) can systematically be truncated to the level of C-particle expectation values,

$$i\hbar\frac{\partial}{\partial t}\langle\hat{C}\rangle = F_{\text{free}}[\langle\hat{C}\rangle] + F_{\text{hier}}[\langle\hat{C}+1\rangle_{1\cdots C}], \tag{12}$$

because any $(C+1)$-particle expectation value is then expressed in terms of the cluster factorization scheme (11). Furthermore, one can describe the dynamics of any $\langle\hat{N}\rangle$ entirely via the lower-order C-particle correlations applied together with Eq. (10). Since the cluster-expansion scheme systematically truncates both the quantum-optical and the many-body hierarchy problem, it constitutes an attractive approach to investigate quantum-optical effects in solids. Several of the Coulomb-induced many-body effects and their systematic solutions are discussed in Ref. [36]. In this paper, our major focus is to explore how different quantum-optical fields and their correlations are described with a finite number of clusters.

C. Explicit form of correlated clusters for boson fields

We assume that the multimode light field has formally $\mathcal{M}$ modes and we know all the normally ordered expectation values,

$$I^{J_1\cdots J_\mathcal{M}}_{K_1\cdots K_\mathcal{M}} \equiv \langle[\hat{B}^\dagger_{\mathbf{q}_1}]^{J_1}\cdots[\hat{B}^\dagger_{\mathbf{q}_\mathcal{M}}]^{J_\mathcal{M}}[\hat{B}_{\mathbf{q}_\mathcal{M}}]^{K_\mathcal{M}}\cdots[\hat{B}_{\mathbf{q}_1}]^{K_1}\rangle \tag{13}$$

for all combinations of $J_j=0,1,2,\ldots$ and $K_k=0,1,2,\ldots$, where the modes $\mathbf{q}_j$ and $\mathbf{q}_k$ $(j\neq k)$ are assumed to be different. Depending on the problem analyzed, the number of modes $\mathcal{M}$ does not have to be finite. At this point, we use $I^{J_1,\ldots,J_\mathcal{M}}_{K_1,\ldots,K_\mathcal{M}}$ axiomatically as one possible presentation of the quantum statistics while we rigorously prove the validity of this assumption later in Sec. IV for single-mode fields.

The conversion of expectation values into clusters can be performed explicitly by introducing a normally ordered characteristic function for the multimode field,

$$\chi_N(\beta_1,\ldots,\beta_\mathcal{M}) \equiv \langle e^{\Sigma_{j=1}^\mathcal{M}\beta_j\hat{B}_j^\dagger}e^{-\Sigma_{k=1}^\mathcal{M}\beta_k^\star\hat{B}_k}\rangle, \tag{14}$$

where we again simplified the notation $\hat{B}_j=\hat{B}_{\mathbf{q}_j}$. The introduced χ_N is a straightforward generalization of normally ordered characteristic functions that are often used to represent the quantum statistics of a single-mode boson field [37].

Mathematically, χ_N is an analytic function that exists in the vicinity of $\beta_j=0$; especially, $\chi_N=1$ for $\beta_j=0$, $\forall j$. Thus, one can perform a Taylor expansion of χ_N around $\beta_j=0$,

$$\chi_N(\beta_1,\ldots,\beta_\mathcal{N}) = \prod_{j=1}^\mathcal{M}\left(\sum_{J_j,K_j=0}^\infty\frac{(-1)^{K_j}}{J_j!K_j!}\beta_j^{J_j}[\beta_j^\star]^{K_j}\right)I^{J_1\cdots J_\mathcal{M}}_{K_1\cdots K_\mathcal{M}}. \tag{15}$$

For classical fields, we find $I^{J_1\cdots J_\mathcal{M}}_{K_1\cdots K_\mathcal{M}}=\Pi_{j=1}^\mathcal{M}\langle\hat{B}_j^\dagger\rangle^{J_j}\langle\hat{B}_j\rangle^{K_j}$ according to Eq. (8). By inserting this into Eq. (15), we observe that the characteristics of classical fields simplifies into

$$\chi_N(\beta_1,\ldots,\beta_\mathcal{N})_S = \exp\left(\sum_{j=1}^\mathcal{M}\beta_j\langle\hat{B}_j^\dagger\rangle - \beta_j^\star\langle\hat{B}_j\rangle\right), \tag{16}$$

where the relevant singlet contributions appear in the exponent.

This observation holds more generally. The correlated clusters can always be identified by

$$\begin{aligned}\chi_N(\beta_1,\ldots,\beta_\mathcal{N}) &= \exp[\xi_N(\beta_1,\ldots,\beta_\mathcal{N})] \Leftrightarrow \xi_N(\beta_1,\ldots,\beta_\mathcal{N})\\ &= \ln[\chi_N(\beta_1,\ldots,\beta_\mathcal{N})],\end{aligned} \tag{17}$$

where ξ_N is the correlation-generating function. More specifically, ξ_N is an analytic function that exists in the vicinity of $\beta_j=0$. The Taylor expansion of ξ_N uniquely defines the correlated clusters through

$$\xi_N(\beta_1,\ldots,\beta_\mathcal{N}) = \prod_{j=1}^\mathcal{M}\left(\sum_{J_j,K_j=0}^\infty\frac{(-1)^{K_j}}{J_j!K_j!}\beta_j^{J_j}[\beta_j^\star]^{K_j}\right)\Delta I^{J_1\cdots J_\mathcal{M}}_{K_1\cdots K_\mathcal{M}}. \tag{18}$$

One can show that the Taylor-expansion coefficients,

$$\Delta I^{J_1\cdots J_\mathcal{M}}_{K_1\cdots K_\mathcal{M}} \equiv \Delta\langle[\hat{B}^\dagger_{\mathbf{q}_1}]^{J_1}\cdots[\hat{B}^\dagger_{\mathbf{q}_\mathcal{M}}]^{J_\mathcal{M}}[\hat{B}_{\mathbf{q}_\mathcal{M}}]^{K_\mathcal{M}}\cdots[\hat{B}_{\mathbf{q}_1}]^{K_1}\rangle, \tag{19}$$

correspond exactly to the correlated clusters that are recursively identified via Eq. (10). The characteristic and correlation-generation functions always allow us to evaluate specific expectation values via a simple differentiation,

$$\begin{aligned}I^{J_1\cdots J_\mathcal{M}}_{K_1\cdots K_\mathcal{M}} &= \prod_{j=1}^\mathcal{M}\left[\frac{\partial^{J_j+K_j}}{\partial\beta_j^{J_j}\partial[-\beta_j^\star]^{K_j}}\right]\chi_N(\beta_1,\ldots,\beta_\mathcal{N})\Bigg|_{\beta_k=0,\ \forall k},\\ \Delta I^{J_1\cdots J_\mathcal{M}}_{K_1\cdots K_\mathcal{M}} &= \prod_{j=1}^\mathcal{M}\left[\frac{\partial^{J_j+K_j}}{\partial\beta_j^{J_j}\partial[-\beta_j^\star]^{K_j}}\right]\xi_N(\beta_1,\ldots,\beta_\mathcal{N})\Bigg|_{\beta_k=0}.\end{aligned} \tag{20}$$

These properties make both χ and ξ convenient functions to present the quantum statistics.

The definition of correlations, Eqs. (17) and (18), is formally identical to the steps needed to determine cumulants for classical distribution functions [56,57]. Thus, one often refers to the cluster expansion as the cumulant expansion. However, the quantum-mechanical generalization of the tra-

ditional cumulant expansion requires an inclusion of complex-valued averages and correlations (cumulants). In addition, the quantum-mechanical correlations can be associated with physical correlations among particles, as shown in Sec. II B.

III. QUANTUM STATISTICS OF A SINGLE-MODE LIGHT FIELD

To explore the applicability of the cluster-expansion approach in quantum-optical problems, we now focus on the standard single-mode analysis, which already allows us to introduce and understand most of the quantum-optical effects. In particular, we want to show how the cluster expansion describes the quantum statistics and to identify the needed finite number of clusters. It is always one of our goals to express the quantum statistics with the minimum number of essential clusters.

The generic cluster-expansion description, provided by Eqs. (13)–(19), can be limited to the single-mode case simply by setting the number of modes $\mathcal{M}$ to one. In practice, for example, balanced-homodyne detection (BHD) [58,59] is capable of extracting exactly one mode out of the multimode field. This measurement technique can be formulated via the transformation [60]

$$\hat{B} = \frac{c\mathcal{S}}{i}\sqrt{\frac{2\epsilon_0}{\hbar\bar{\omega}}}\int dt\phi^{\star}(t)\hat{E}(t), \tag{21}$$

where $\bar{\omega}$ is the central frequency related to the mode, and the detectors collect the incoming source field $\hat{E}(t)$ in the area $\mathcal{S}$. This particular transformation is appropriate for a situation where a beam splitter is used to mix $\hat{E}(t)$ with a well-defined classical laser pulse, the local oscillator, having a single temporal mode $\phi^{\star}(t)$. When the split signals are detected with two detectors, the difference of the output signals can be related to one single temporal mode $\hat{B}$, projected through the local oscillator out of the characterized source field, according to Eq. (21). By choosing $\phi(t)=\frac{1}{\sqrt{\mathcal{V}}}e^{-i\omega_{\mathbf{q}}t}$, for instance, the BHD picks up a single mode $\hat{B}=\hat{B}_{\mathbf{q}}$ in the propagation direction determined by the measurement setup. This formulation can easily be extended to include the polarization dependence and/or geometric aspects of the detection, as is done, e.g., in Ref. [61].

A. Equivalent representations of quantum statistics

Since Eq. (21) identifies how single-mode fields can be retrieved from multimode light, we can now concentrate on the analysis of an arbitrary single-mode field. As the only essential feature, we have to remember that $\hat{B}$ is a bosonic operator with the usual commutation relations. As the next step, we connect the *expectation-value representation*,

$$I_K^J \equiv \langle[\hat{B}^{\dagger}]^J[\hat{B}]^K\rangle, \quad J \text{ and } K \text{ integers}, \tag{22}$$

with other quantum-statistical descriptions. Generally, we can introduce the quantum statistics via the density matrix in the complete and orthogonal basis of quantum states. For quantized light, we can choose the Fock-state basis $|n\rangle$ that defines the density matrix,

$$\hat{\rho} = \sum_{n,m}|n\rangle C(n,m)\langle m|, \quad n \text{ and } m \text{ integers}, \tag{23}$$

where the complex-valued coefficients $C(n,m)$ determine the specific structure of $\hat{\rho}$. The diagonal elements $C(n,n)$ define the photon statistics that contains only a reduced amount of information with respect to the level of the full quantum statistics.

The algebraic properties of the Fock state produce

$$[\hat{B}^{\dagger}]^J|n\rangle = \sqrt{\frac{(n+J)!}{n!}}|n+J\rangle, \quad \hat{B}^K|n\rangle = \sqrt{\frac{n!}{(n-K)!}}|n-K\rangle. \tag{24}$$

By presenting the appearing factorials through the Γ function, one realizes that $\frac{n!}{(n-K)!}$ correctly vanishes for $K>n$. These relations also produce a one-to-one mapping between I_K^J and $\hat{\rho}$ according to

$$I_K^J = \sum_{n=0}^{\infty}\frac{\sqrt{(n+J)!(n+K)!}}{n!}C(n+K,n+J) \Leftrightarrow C(n,m)$$
$$= \frac{1}{\sqrt{n!m!}}\sum_{K=0}^{\infty}\frac{(-1)^K}{K!}I_{K+n}^{K+m}. \tag{25}$$

This mapping relation is strictly valid for quantum-optical fields that are limited in photon number to be below N_{lim}, i.e., $C(n,m)=0$ for $n,m\geqslant N_{\mathrm{lim}}$. Since N_{lim} can be arbitrarily large but finite, these states constitute a large subset of all possible quantum-optical states. However, the relation (25) can produce a mathematically indefinite value for $C(n,m)$ for some quantum-optical states with $N_{\mathrm{lim}}\to\infty$. This problem is addressed later in Sec. IV B and the convergence problem is solved in Secs. IV C–IV E through the cluster-expansion approach. Especially, the one-to-one correspondence of the expectation-value representation and density matrix is then generally justified such that I_K^J and $\hat{\rho}$ provide an equivalent description of quantum statistics. One also can write $C(n,m)=\frac{1}{\sqrt{n!m!}}\langle:[\hat{B}^{\dagger}]^m e^{-\hat{B}^{\dagger}\hat{B}}[\hat{B}]^n:\rangle$, where $:\hat{O}:$ orders all creation operators in a generic operator sequence $\hat{O}$ to the left. The resulting formal expression can be used as a starting point of the quantum theory of photodetection [62,63].

The connection of the cluster expansion with I_K^J and $\hat{\rho}$ follows from Eqs. (14) and (17) leading to

$$\chi_N(\beta) \equiv \langle e^{\beta\hat{B}^{\dagger}}e^{-\beta^{\star}B}\rangle = \sum_{J,K=0}^{\infty}\frac{\beta^J(-\beta^{\star})^K}{J!K!}I_K^J = e^{\xi_N(\beta)},$$
$$\xi_N(\beta) = \sum_{J,K=0}^{\infty}\frac{\beta^J(-\beta^{\star})^K}{J!K!}\Delta I_K^J = \ln[\chi_N(\beta)] \tag{26}$$

for the normally ordered characteristics and correlation-generating functions, respectively. Both of these functions exist and are analytic in the vicinity of $\beta=0$, with $\chi_N(0)=1$ and $\xi_N(0)=0$. Due to the uniqueness of the Taylor expansion, χ_N, ξ_N, and I_K^J (or $\hat{\rho}$) are equivalent representations of quan-

tum statistics. Especially, χ_N and ξ_N can be converted to the other with a straightforward one-to-one mapping, $\chi_N(\beta)=e^{\xi_N(\beta)}$.

B. The Wigner function

We introduce the quadrature operators for the quantized single-mode light field,

$$\hat{x}=\frac{\hat{B}+\hat{B}^\dagger}{2},\quad \hat{y}=\frac{\hat{B}-\hat{B}^\dagger}{2i}. \tag{27}$$

Using the bosonic commutation relations, we obtain $[\hat{x},\hat{y}]_-=\frac{i}{2}$, $[\hat{x},\hat{x}]_-=0=[\hat{y},\hat{y}]_-$ Thus, the choice of Eq. (27) allows us to interpret $\hat{x}$ to correspond to a position while $\hat{y}$ is analogous to a momentum of a particle. The simultaneous measurement of the $\hat{x}$ and $\hat{y}$ quadratures is governed by the Heisenberg uncertainty relation,

$$\Delta\langle\hat{x}\rangle^2\equiv\langle\hat{x}^2\rangle-\langle\hat{x}\rangle\langle\hat{x}\rangle,\quad \Delta\langle\hat{y}\rangle^2\equiv\langle\hat{y}^2\rangle-\langle\hat{y}\rangle\langle\hat{y}\rangle,$$

$$\Delta\langle\hat{x}\rangle\Delta\langle\hat{y}\rangle\geqslant\frac{1}{4}, \tag{28}$$

which sets the ultimate limit to the accuracy for the detection of electromagnetic fields.

The density matrix of the field can be presented more explicitly using the position or momentum representation of $\hat{\rho}$. In other words, we may use $\rho(x,x')=\langle x|\hat{\rho}|x'\rangle=\Sigma_{n,m}C(n,m)\psi_n(x)\psi_m^\star(x')$, where $\psi_n(x)$ are the usual harmonic-oscillator wave functions in the real-space representation. One can also compute the Wigner function [23,64] with the help of the Fourier transformation,

$$W(x,y)=\frac{1}{\pi}\int dr\rho\left(x+\frac{r}{2},x-\frac{r}{2}\right)e^{-i2yr}. \tag{29}$$

In general, $W(x,y)$ is a real-valued function in the xy phase space.

We notice that there is a one-to-one mapping between $W(x,y)$ and the density matrix via the Fourier transform and its inverse. Thus, $W(x,y)$, $\hat{\rho}$, I_K^J, and ΔI_K^J yield equivalent presentations of the quantum statistics.

By introducing the complex number

$$\alpha\equiv x+iy,\quad \Leftrightarrow x=\frac{\alpha+\alpha^\star}{2},\quad \text{and } y=\frac{\alpha-\alpha^\star}{2i} \tag{30}$$

and using Eq. (29), one finds another standard form of the Wigner function [2,23],

$$W(\alpha)=\frac{1}{\pi^2}\int d^2\beta\chi_N(\beta)e^{-|\beta|^2/2}e^{\beta^\star\alpha-\beta\alpha^\star}. \tag{31}$$

Here, the integration is performed over the complex plane, e.g., $d^2\beta=d\beta_1 d\beta_2$ with $\beta=\beta_1+i\beta_2$. In the last step, we can identify the normally ordered characteristic function with the help of Eq. (26).

C. Marginal distributions

Since the Wigner function is defined in the two-dimensional xy plane, it is often convenient to introduce a rotated Wigner function,

$$W_\theta(\tilde{\alpha}_1,\tilde{\alpha}_2)=W_\theta(\tilde{\alpha})\equiv W(\tilde{\alpha}e^{i\theta})=W(\alpha),\quad \alpha\equiv\tilde{\alpha}e^{i\theta}. \tag{32}$$

This allows us to define the general marginal distribution in any arbitrary direction,

$$P_\theta(\tilde{\alpha}_1)=\int d\tilde{\alpha}_2 W_\theta(\tilde{\alpha}),\quad \tilde{\alpha}=\tilde{\alpha}_1+i\tilde{\alpha}_2. \tag{33}$$

It is straightforward to show that $P_{\theta=0}(x)=\langle x|\hat{\rho}|x\rangle$ and $P_{\theta=\pi/2}(y)=\langle y|\hat{\rho}|y\rangle$ produces probability distributions for position and momentum quadratures, respectively. These marginal distributions are always positive valued such that they allow for the usual probabilistic interpretation.

To have a convenient description of rotated quadrature quantities, we introduce rotated boson and quadrature operators according to

$$\hat{B}_\theta\equiv Be^{-i\theta},\quad \hat{x}_\theta\equiv\frac{\hat{B}_\theta+\hat{B}_\theta^\dagger}{2}=\cos\theta\hat{x}+\sin\theta\hat{y},$$

$$\hat{y}_\theta\equiv\frac{\hat{B}_\theta-\hat{B}_\theta^\dagger}{2i}=-\sin\theta\hat{x}+\cos\theta\hat{y}. \tag{34}$$

These quadratures obey the relations,

$$\hat{y}_\theta=\hat{x}_{\theta+(\pi/2)},\quad [\hat{x}_\theta,\hat{y}_\theta]_-=\frac{i}{2},\quad [\hat{x}_\theta,\hat{x}_\theta]_-=0=[\hat{y}_\theta,\hat{y}_\theta]_-, \tag{35}$$

such that any two perpendicular quadratures constitute a canonical pair. In other words, the accuracy of measurements in $\hat{x}_\theta$ and $\hat{x}_{\theta+\pi/2}$ is limited by the Heisenberg uncertainty limit (28). In this context, we notice that that specific distinction of position and momentum coordinates is not relevant for quantum-optical fields such that it is more meaningful to discuss quadrature quantities in a given direction.

It is a specialty of the BHD setup that it directly detects that quadrature x_θ of the signal in the direction θ that is controllable via the local-oscillator phase. In particular, the ensemble average of the BHD measurements produces

$$\langle x_\theta\rangle=\int dx_\theta x_\theta P_\theta(x_\theta). \tag{36}$$

If one makes a statistical analysis of the outcomes obtained via repetition, the counting statistics actually constructs $P_\theta(x_\theta)$ if the size of the measurement ensemble is large enough. As shown by Vogel and Risken [65], the Wigner function behind the marginal distribution can be solved by inverting Eq. (33). This well-known problem leads to the Radon transformation [65]

$$W(\alpha)=\frac{2}{\pi^2}\int_0^\pi d\theta\int_0^\infty rdr\int_{-\infty}^\infty dxP_\theta(x)\cos 2r(x-\alpha_1\cos\theta-\alpha_2\sin\theta). \tag{37}$$

Thus, all measurements related to Eq. (36) can be directly applied to construct the quantum statistics as demonstrated in the pioneering work of Smithey *et al.* [60].

IV. CLUSTER-EXPANSION REPRESENTATION IN QUANTUM OPTICS

By using the definition (33) and by taking an inverse Fourier transformation of Eq. (31), a straightforward derivation produces the one-to-one mappings

$$\chi_N(\beta) = e^{|\beta|^2/2} \int d^2\alpha W(\alpha) e^{-\beta^\star \alpha + \beta \alpha^\star}$$

$$\Leftrightarrow W(\alpha) = \frac{1}{\pi^2} \int d^2\beta \chi_N(\beta) e^{-|\beta|^2/2} e^{\beta^\star \alpha - \beta \alpha^\star}, \tag{38}$$

$$\chi_N^\theta(iq) \equiv \chi_N(iqe^{i\theta}) = e^{(1/2)q^2} \int_{-\infty}^{\infty} dx P_\theta(x) e^{+2iqx}$$

$$\Leftrightarrow P_\theta(x) = \frac{1}{\pi} \int dq \chi_N^\theta(iq) e^{-q^2/2} e^{-2iqx} \tag{39}$$

between the expectation-value representation and $P_\theta(x)$ or $W(\alpha)$. Since both the Wigner function and the marginal distributions $P_\theta(x)$ represent the quantum statistics of light in a form that is accessible in experiments, we derive next the explicit steps needed to convert the phase-space representation into the corresponding expectation-value and cluster-expansion forms and vice versa. The resulting relations nicely show how efficiently the cluster-expansion technique can be applied to describe and identify quantum-optical properties.

A. From phase space to expectation-value representation

If we assume that the Wigner function is known, we may apply (38) directly to evaluate I_K^J. More specifically, we Taylor expand the function $e^{-\beta^\star \alpha + \beta \alpha^\star}$ in terms of β and $\beta^\star$ to find

$$\chi_N(\beta) = e^{|\beta|^2/2} \sum_{J,K=0}^{\infty} \frac{\beta^J [-\beta^\star]^K}{J!K!} \langle \alpha \rangle_K^J,$$

$$\langle \alpha \rangle_K^J \equiv \int d^2\alpha W(\alpha) [\alpha^\star]^J \alpha^K, \tag{40}$$

where we have identified the expectation values $\langle \alpha \rangle_K^J$ that simply describe the different moments of the Wigner function. If we now Taylor expand also the $e^{|\beta|^2/2}$ part in Eq. (40), we obtain

$$\chi_N(\beta) = \sum_{J,K=0}^{\infty} \frac{\beta^J [-\beta^\star]^K}{J!K!} \times \sum_{L=0}^{\max(J,K)} \frac{J!K!}{(J-L)!(K-L)!L!} \left(-\frac{1}{2}\right)^L \langle \alpha \rangle_{K-L}^{J-L} \tag{41}$$

after we have properly rearranged the sums. By comparing this result with the definition (26) of the characteristics function, we conclude that the expectation-value representation is given by

$$I_K^J = \sum_{L=0}^{\max(J,K)} \frac{J!K!}{(J-L)!(K-L)!L!} \left(-\frac{1}{2}\right)^L \langle \alpha \rangle_{K-L}^{J-L},$$

$$\langle \alpha \rangle_K^J \equiv \int d^2\alpha W(\alpha) [\alpha^\star]^J \alpha^K, \tag{42}$$

where we have repeated the definition of $\langle \alpha \rangle_K^J$ for the sake of completeness. Since all $\langle \alpha \rangle_K^J$ are finite for any physical Wigner function (see also the discussion in Sec. V) and the transformation (42) has only a finite number of terms, the Wigner function can always be converted into the expectation-value representation without any numerical convergence problem.

In many physically relevant situations, one often knows the distributions $P_\theta(x)$ instead of $W(\alpha)$. To convert $P_\theta(x)$ into the expectation-value representation, we apply the same strategy as for the Wigner function. We Taylor expand e^{+2iqx} in Eq. (39) to produce

$$\chi_N^\theta(iq) \equiv \chi_N(iqe^{i\theta}) = e^{(1/2)q^2} \sum_{J=0}^{\infty} (iq)^J \langle (2\bar{x})^J \rangle$$

$$= \sum_{J=0}^{\infty} (iq)^J \sum_{K=0}^{[J/2]} \frac{\langle (2\bar{x}_\theta)^{J-2K} \rangle}{(-2)^K K!}, \tag{43}$$

$$\langle (2\bar{x}_\theta)^j \rangle \equiv \int_{-\infty}^{\infty} dx \frac{(2x)^j}{j!} P_\theta(x), \tag{44}$$

where we identified the normalized quadrature moments $\langle (2\bar{x}_\theta)^j \rangle$. The Taylor expanded part, $e^{(1/2)q^2}$, yields the final form after proper reorganization of the appearing sums. Here, we have used the notation convention $[\frac{L}{2}]$, where the term within the brackets is truncated to the nearest lowest integer such that

$$\left[\frac{L}{2}\right] = \begin{cases} \dfrac{L}{2} & \text{for even } L \\ \dfrac{L-1}{2} & \text{for odd } L \end{cases} \tag{45}$$

always gives an integer-valued result.

To convert $\chi_N^\theta(y)$ into a similar series-expansion format, we rearrange the sums in Eq. (26) as follows:

$$\chi_N(iqe^{i\theta}) = \sum_{J,K=0}^{\infty} \frac{e^{i\theta(J-K)}}{J!K!} I_K^J (iq)^{J+K} \equiv \sum_{J=0}^{\infty} (iq)^J I_{\Sigma,J}^\theta, \tag{46}$$

$$I_{\Sigma,J}^\theta \equiv \sum_{L=0}^{J} \frac{e^{i\theta(2L-J)}}{L!(J-L)!} I_{J-L}^L. \tag{47}$$

We notice now that $I_{\Sigma,K}^\theta$ is a *collective K-particle expectation value* since it contains all different I_L^J with $J+L=K$. This observation becomes vitally important in Sec. VI where we investigate how quantum statistically corrupted distributions can be restored to their true original form. If we now compare Eq. (43) with Eq. (46), we recognize that marginal dis-

tributions can be converted into collective K-particle expectation values via

$$I^{\theta}_{\Sigma,L} = \sum_{K=0}^{[L/2]} \frac{\langle (2\bar{x}_\theta)^{L-2K} \rangle}{(-2)^K K!}, \quad \langle (2\bar{x}_\theta)^j \rangle \equiv \int_{-\infty}^{\infty} dx \frac{(2x)^j}{j!} P_\theta(x). \tag{48}$$

In other words, we have explicitly defined how $P_\theta(x)$ is converted into the expectation-value representation. In the same way as Eq. (42), the transformation from $I_{\Sigma,J}$ to $P(x)$ contains only a finite number of terms. Thus, P can always be converted into collective expectation values without numerical problems.

To illustrate how $I^{\theta}_{\Sigma,L}$ and $\langle (2\bar{x}_\theta)^j \rangle$ describe the quantum statistics, we analyze them for a few exemplary sources. For a given Fock state $|n\rangle$, all quadrature directions produce a probability distribution

$$P_n(x) = |\langle x|n\rangle|^2 = \frac{1}{2^n n!} [H_n(\sqrt{2}x)]^2 \sqrt{\frac{2}{\pi}} e^{-2x^2}, \tag{49}$$

where $H_n(x)$ is the Hermite polynomial. A coherent state has a marginal distribution of a displaced vacuum

$$P_{\mathrm{coh}}(x) = \sqrt{\frac{2}{\pi}} e^{-2(x-X)^2}, \tag{50}$$

where the center of the distribution, X, depends on the quadrature direction analyzed. Besides being displaced, the vacuum state can additionally be either stretched or squeezed. When all quadrature directions produce the same width of the distribution,

$$P_{\mathrm{ther}}(x) = \sqrt{\frac{2}{\pi(1+2n_{\mathrm{th}})}} e^{-2(x^2/1+2n_{\mathrm{th}})}, \tag{51}$$

the characterized field has a thermal quantum statistics where the thermal parameter n_{th} defines the average number of photons. Alternatively, the coherent field can be squeezed to have a width ΔX such that

$$P_{\mathrm{sqz}}(x) = \sqrt{\frac{1}{2\pi\Delta X^2}} e^{-(x-X)^2/2\Delta X^2}, \tag{52}$$

where both X and ΔX depend on the quadrature direction. These four field types represent the basic quantum-statistical fields in quantum optics; see e.g., Ref. [2].

The shaded area in Fig. 2(a) displays the thermal distribution with $n_{\mathrm{th}}=2$ photons on average, in Fig. 2(c) a coherent state with the displacement $X=\sqrt{2}$, in Fig. 2(e) a squeezed state with $X=\sqrt{2}$ and a four-times narrower distribution than the vacuum, and in Fig. 2(g) the Fock-state $|2\rangle$, respectively. The corresponding $\langle [2\bar{x}]^J \rangle$ (red squares) and $I_{\Sigma,J}$ (black circles) values are computed with Eq. (48) and shown in the right column. To distinguish the different index values, open symbols indicate even J while filled symbols denote odd J. The connecting lines just serve as a guide to the eye.

For both the thermal and the Fock state, all odd $\langle [2\bar{x}]^{2J+1} \rangle$ quantities vanish. In this situation, also the odd collective expectation values $I_{\Sigma,2J+1}$ remain zero, which is a general property of any symmetric distribution as can be concluded

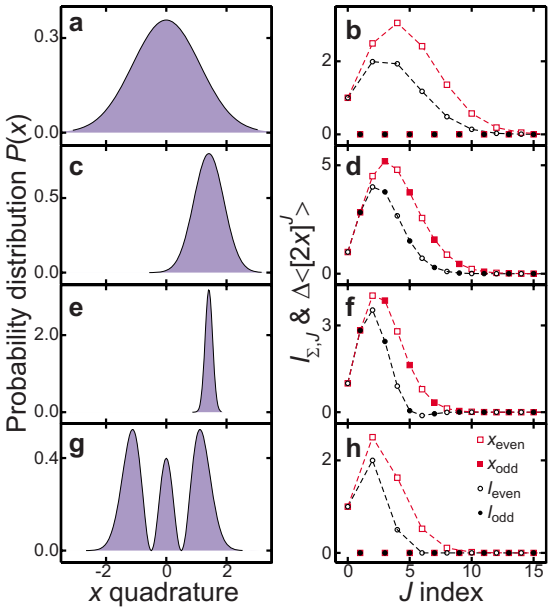

FIG. 2. (Color online) Quadrature distributions vs expectation-value representation. Different input distributions (shaded areas, left column) are compared with the corresponding $\langle [2\bar{x}]^J \rangle$ (red squares, right column) and $I_{\Sigma,J}$ (black circles, right column). The lines are guides to the eye. The quantum statistics of (a), (b) thermal; (c), (d) coherent; (e), (f) squeezed; and (g), (h) Fock state $|2\rangle$ are analyzed.

from Eq. (48). For the displaced coherent- and squeezed-state distributions, however, the even and odd contributions have similar values and seem to follow a "continuous" curve.

As a common property of all of the distributions investigated, we note that both $\langle [2\bar{x}]^J \rangle$ and $I_{\Sigma,J}$ decay rapidly for elevated J. At the same time, $I_{\Sigma,J}$ decreases faster than $\langle [2\bar{x}]^J \rangle$. These observations illustrate that the expectation-value representation can be applied to describe the quantum statistics with a reduced number of quantities. In particular, the strongly decaying $I_{\Sigma,J}$ suggests that the originally infinite-dimensional quantum statistics can rather accurately be described using only a finite number of parameters. In the following, we will show that the cluster expansion allows us to find an efficient way to express the quantum statistics with the minimum number of physically relevant correlations.

Besides these common properties, we observe in Fig. 2 a few distinct features for the squeezed and the Fock states, which are both generally considered to possess strong quantum characteristics. The Fock state $|2\rangle$ displays strictly vanishing $I_{\Sigma,J}$ above $J=4$. Mathematically this follows from the fact that any $J \geqslant 5$ particle operator, i.e., $\langle 2|[B^+]^{J-L}B^L|2\rangle$, involves more than two destruction operators acting on a two-photon state which automatically provides a vanishing result. If we now follow $I_{\Sigma,J}$ of the squeezed state, we observe that $I_{\Sigma,J}$ is slightly negative around $J=6$. In general, both negative $I_{\Sigma,J}$ and an abrupt transition to vanishing $I_{\Sigma,J}$ indicate that the characterized source exhibits genuine quantum features.

B. From expectation-value to phase-space representation

Since we can construct the expectation-value representation whenever either the Wigner function or the marginal

distributions are known, it is natural to seek the inverse transformation. To explicitly evaluate $P_\theta(x)$ or $W(\alpha)$ when I_K^J is known, we simply substitute the Taylor expanded form (26) into Eqs. (38) yielding

$$W(\alpha) = \sum_{J,K=0}^{\infty} (-1)^K I_K^J w_K^J(\alpha), \tag{53}$$

where we have identified

$$w_K^J(\alpha) \equiv \frac{1}{\pi^2 J! K!} \int d^2\beta \beta^J (\beta^\star)^K e^{-|\beta|^2/2} e^{+\beta^\star \alpha - \beta \alpha^\star}$$
$$= \frac{2}{\pi} e^{-2|\alpha|^2} \sum_{j=0}^{\max(J,K)} \frac{2^{J+K-j} \alpha^{J-j} [-\alpha^\star]^{K-j}}{j!(J-j)!(K-j)!} \tag{54}$$

following from the explicit evaluation of the Gaussian integral. A similar explicit transformation from expectation values to marginal distributions is obtained by inserting Eq. (46) into Eq. (39). As a result, the collective K-particle expectation value is expressed as

$$P_\theta(x) = \sum_{J=0}^{\infty} I_{\Sigma,J}^\theta p^{(J)}(x), \tag{55}$$

where we identified

$$p^{(K)}(x) \equiv \frac{1}{\pi} \int dy (iy)^K e^{-(1/2)y^2 - 2ixy}$$
$$= \frac{1}{\sqrt{2\pi}} e^{-(1/2)x^2} \sum_{J=0}^{[K/2]} \frac{K!}{J!(K-2J)!} \frac{x^{K-2J}}{(-2)^J}, \tag{56}$$

which follows after a straightforward Gaussian integration. We now notice that the conversion from I_K^J into the phase-space distributions requires a summation over infinitely many elements, unlike the inverse transformations (42) and (48). Thus, Eqs. (53) and (55) may yield divergences, especially when they are implemented numerically.

In order to work around this problem, we next investigate the stability of the transformations for I_K^J into more traditional representations of the quantum statistics. For this purpose, we use thermal light as one of the simplest examples where [36]

$$I_K^J = \delta_{J,K} J! [n_{\rm th}]^J, \tag{57}$$

and $n_{\rm th}$ is the average number of photons in the thermal state. This, together with Eqs. (53) and (55), produces

$$W(\alpha) = \sum_{J=0}^{\infty} (-n_{\rm th})^J J! w_J^J(\alpha),$$

$$P_\theta(x) = \sum_{K=0}^{\infty} [n_{\rm th}]^K p^{(2K)}(x). \tag{58}$$

Based on Eq. (54), we have $w_J^J(0) = \frac{2^{J+1}}{\pi J!}$, such that

$$W_{\rm th}(0) = \frac{2}{\pi} \lim_{K\to\infty} \sum_{J=0}^{K} (-2n_{\rm th})^J = \frac{2}{\pi} \lim_{K\to\infty} \frac{1-(-2n_{\rm th})^{K+1}}{1+2n_{\rm th}}, \tag{59}$$

where we have used the finite form of the geometric series. This relation converges to

$$W_{\rm th}(0) = \frac{2}{\pi} \frac{1}{1+2n_{\rm th}}, \tag{60}$$

only if $n_{\rm th} < \frac{1}{2}$. This example demonstrates that the direct transformation from the expectation-value to the Wigner-function representation can occasionally be numerically divergent. Nonetheless, the Taylor expansion of Eq. (60) uniquely yields the same expansion as in Eq. (59). Thus, the functional identification via Eqs. (59) and (60) still works as a consequence of the uniqueness of the representations. After a straightforward calculation, one eventually finds the convergence to

$$W(\alpha) = \frac{2}{\pi(1+2n_{\rm th})} e^{-2|\alpha|^2/(1+2n_{\rm th})} \quad \text{when } n_{\rm th} < \frac{1}{2},$$

$$P_\theta(x) = \sqrt{\frac{2}{\pi(1+2n_{\rm th})}} e^{-2x^2/(1+2n_{\rm th})} \quad \text{when } n_{\rm th} < \frac{1}{2}. \tag{61}$$

These are the well-known quantum-statistical forms of the thermal state. Nonetheless, for large $n_{\rm th}$ this identification can be made only formally and the numerical evaluations of sums (59) yield a diverging result. Besides this, we also notice that Eq. (59) actually converges rapidly whenever $n_{\rm th}$ is small. The $n_{\rm th}=0$ case actually shows extreme convergence where already the first I_0^0 term produces the correct result because the thermal state in this case is just a vacuum. This intriguing property can be fully utilized after we consider the cluster-expansion representation of quantum-optical fields.

The possibility to have to deal with potentially divergent transformations is clearly undesirable. Thus, we need to find an alternative scheme where both the identification of functional forms and the numerical implementation of the transformation yield uniquely convergent expressions. As we will demonstrate in Sec. IV D, this objective is reached by involving clusters in the transformation. However, before we enter into this analysis, we first investigate the transformation (53) for the thermal and the Fock state $|4\rangle$ with

$$I_K^J = \delta_{J,K} \frac{4!}{(4-J)!}. \tag{62}$$

This expectation value vanishes for $J>4$ because $(4-J)!$ diverges for negative values of $(4-J)$ that follow after factorials are presented through the Γ function. Defining

$$W_K(0) = \frac{2}{\pi} \sum_{J=0}^{K} \frac{(-1)^J}{J!} 2^J I_J^J, \tag{63}$$

we introduce the ratio $r_K \equiv \frac{W_K(0)}{W(0)}$, where $W(0)$ is the actual value of the Wigner function.

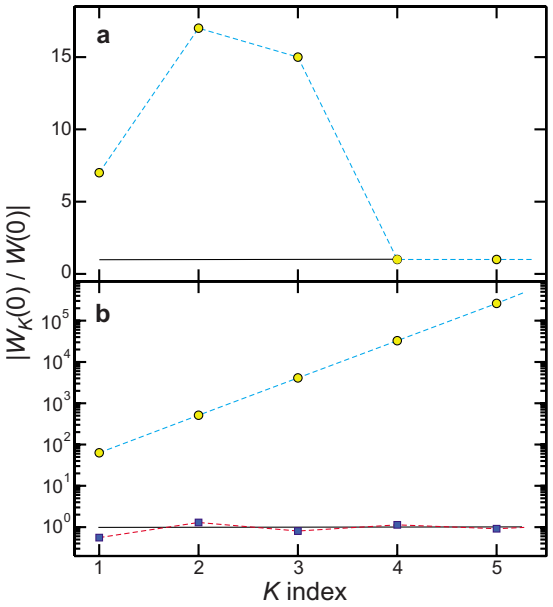

FIG. 3. (Color online) Convergence of the Wigner function via direct implementation. The ratio of the computed $W_K(0)$ [via Eq. (63)] and the actual $W(0)$ is presented as function of K. (a) The Fock state $|4\rangle$ [Eq. (62)] is analyzed together with (b) the thermal state [Eq. (57)] with 4 photons (circles) and $\frac{1}{3}$ photons (squares) on average. The horizontal line indicates the exact result.

Figure 3(a) shows the $r_K \equiv \frac{W_K(0)}{W(0)}$ ratio for the Fock state $|4\rangle$ as a function K. The limit of the exact reconstruction $r_K \rightarrow 1$ is indicated by the solid black line. As can be seen in the figure, we find large deviations for values of K below 4. However, when K exceeds the photon number in the Fock state, there is an abrupt convergence to the exact value, i.e., a very similar transition as already seen in Fig. 2 for the Fock state $|2\rangle$. An analogous convergence sequence actually follows for any Fock state $|N\rangle$ beyond the $2N$-photon expectation values. Thus, a truncation to $2N$-particle expectation values guarantees convergence for any state limited up to the Fock state $|N\rangle$. This approach is commonly used in quantum optics. In other words, mapping from I_K^J to W works as long as the particular quantum statistics involves only a finite number of photon states.

However, this approximation is unsuccessful for many other relevant states such as coherent, squeezed, or thermal states since they contain all possible Fock states. As an example, we evaluate r_K for the thermal states with $n_{\rm th}=4$ (circles) and $n_{\rm th}=\frac{1}{3}$ in Fig. 3(b). We see that the $n_{\rm th}=4$ case diverges away from the exact value (black line) while $n_{\rm th}=\frac{1}{3}$ yields a fast convergence for elevated K. This observation is in full agreement with the convergence limit $2n_{\rm th}<1$. Thus, only thermal fields with a small enough average photon number yield a converging result of $W(r)$ when it is directly evaluated from the I_K^J representation.

Obviously, the thermal state is just one example whose $W(r)$ and $P(r)$ have diverging representations in terms of I_J^J. The criteria for general convergence of the direct scheme can be derived from Eq. (63). This series converges whenever the normalized quantity $\bar{I}_J^J \equiv \frac{2^J I_J^J}{J!}$ decreases as J becomes large enough. For Fock states, $\bar{I}_J^J=0$ for large enough J while $\bar{I}_J^J \rightarrow 0$ ($\bar{I}_J^J \rightarrow \infty$) for thermal light with $2n_{\rm th}<1(2n_{\rm th}>1)$, which identifies the exact same convergence criteria as Eq. (61). The investigated incoherent fields have $I_{\Sigma,2J}=I_J^J$, which generally follows from $I_K^J=\delta_{J,K}I_K^J$ and Eq. (48). Thus, the true convergence of the transformation from expectation-value to phase-space representation can be obtained for the normalized quantities $\bar{I}_J^J$ instead of $I_{\Sigma,J}$ presented in Fig. 2. The general properties of the normalized $\bar{\bar{I}}_{\Sigma,J}$ will be discussed later in Sec. IV D.

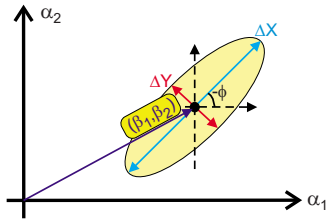

FIG. 4. (Color online) Schematic representation for the contour of a Wigner distribution. The contour for a singlet-doublet field is generally an ellipse that is displaced from the origin to the point (β_1,β_2) indicated by an arrow. This vector defines the direction, i.e., coherent phase, of the field. The quadrature fluctuations can have an independent direction ϕ.

C. Quantum statistics of general singlet-doublet fields

Before we show how correlated clusters can be used in the transformation from expectation-value to phase-space representation, we want to determine the importance of correlated clusters for quantum-optical fields. For this purpose, we start with the singlet-doublet fields, i.e., light whose quantum statistics involves maximally ($C=2$)-particle correlations. More mathematically, the correlation-generating function (26) follows then from

$$\xi_N^{\rm SD}(\beta) = \langle \hat{B}^\dagger \rangle \beta - \langle B \rangle \beta^\star - \Delta\langle \hat{B}^\dagger B \rangle |\beta|^2 + \frac{\Delta\langle \hat{B}^\dagger \hat{B}^\dagger \rangle}{2}\beta^2 + \frac{\Delta\langle BB \rangle}{2}(\beta^\star)^2, \tag{64}$$

which defines the characteristic function via $\chi_N^{\rm SD}(\beta)=e^{\xi_N^{\rm SD}(\beta)}$. We can also analyze the singlet-doublet factorization in the quadrature direction θ yielding

$$\xi_{N,\theta}^{\rm SD}(iq) \equiv \xi_N^{\rm SD}(iqe^{i\theta}) = 2i\langle \hat{x}_\theta \rangle q - 2q^2\left[\Delta\langle \hat{x}_\theta^2 \rangle - \frac{1}{4}\right], \tag{65}$$

according to the definitions (28) and (34). We notice again that $\xi^{\rm SD}$ is directly related to the displacement and squeezing of a given quadrature. As we will see later, this format becomes particularly useful once we construct marginal distributions using clusters.

We next consider an ansatz for the density matrix,

$$\hat{\rho}_{\rm SD} \equiv D(\alpha)S(\gamma)\hat{\rho}_{\rm th}(n_{\rm th})S^\dagger(\gamma)D^\dagger(\alpha), \tag{66}$$

that produces exactly $\chi_N^{\rm SD}(\beta)=e^{\xi_N^{\rm SD}(\beta)}$, as shown in Appendix A. This ansatz is fully defined via the displacement and the squeezing operators,

$$D(\alpha) = e^{\alpha \hat{B}^\dagger - \alpha^\star B}, \quad S(\gamma) \equiv e^{(1/2)[\gamma^\star \hat{B}^2 - \gamma \hat{B}^2]}, \tag{67}$$

respectively, together with the density matrix of a thermal state,

$$\hat{\rho}_{\rm th}(N) \equiv \sum_k |k\rangle p_N^{\rm th}(k)\langle k|, \quad p_N^{\rm th}(k) = \frac{1}{1+N}\left(\frac{N}{1+N}\right)^k, \tag{68}$$

where $p_N^{\rm th}(k)$ is the photon statistics. Physically, α, γ, and N correspond to displacement, squeezing, and thermal parameters, respectively. Appendix A shows that by fixing

$$\beta = \langle B\rangle,$$

$$N = 2\left(\Delta X \Delta Y - \frac{1}{4}\right),$$

$$\gamma = \frac{1}{2}\frac{\Delta\langle BB\rangle}{|\Delta\langle BB\rangle|} \ln \frac{\Delta Y}{\Delta X}, \tag{69}$$

we obtain the equivalence between $\hat{\rho}_{\rm SD}$ and $\xi_{\rm SD}$. Here, the thermal and squeezing parameters are defined through the maximum and minimum values for the quadrature fluctuations,

$$\Delta X \equiv \frac{1}{\sqrt{2}}\sqrt{\frac{1}{2} + \Delta\langle \hat{B}^\dagger B\rangle + |\Delta\langle BB\rangle|},$$

$$\Delta Y \equiv \frac{1}{\sqrt{2}}\sqrt{\frac{1}{2} + \Delta\langle \hat{B}^\dagger B\rangle - |\Delta\langle BB\rangle|}, \tag{70}$$

respectively. Note that ΔX (ΔY) is the maximum (minimum) of $\sqrt{\Delta\langle \hat{x}_\theta^2\rangle}$ as θ is scanned from 0 to π. The positivity requirement for the thermal parameter imposes the condition

$$\Delta X \Delta Y \geqslant \frac{1}{4}, \tag{71}$$

which actually is the Heisenberg uncertainty principle defined earlier, Eq. (28).

Altogether, these observations lead to a general interpretation of the parameters defining the singlet-doublet truncation. The singlet contribution, i.e., β defines the classical amplitude of the field. Similarly, the doublets determine ΔX and ΔY, which fulfill the Heisenberg uncertainty relation, while the thermal parameter N defines the degree to which the minimum-uncertainty limit of $\frac{1}{4}$ is exceeded by the quantum field. Once the quadrature fluctuations are different, γ becomes nonzero such that $\ln \frac{\Delta Y}{\Delta X}$ defines the level of squeezing while $\arg[\Delta\langle BB\rangle]$ determines the direction of squeezing. Consequently, *any physical combination of* $\langle \hat{B}\rangle$, $\Delta\langle \hat{B}^\dagger \hat{B}\rangle$, *and* $\Delta\langle \hat{B}\hat{B}\rangle$ *can always be traced back to a singlet-doublet factorization and a physical density matrix of elementary quantum-optical fields*. In general, the manifold of coherent-thermal-squeezed fields is very important in quantum optics since it allows us to analyze properties all the way from classical to truly quantum-mechanical sources. It is interesting to notice that the simple singlet-doublet clusters define these states with a minimum amount of parameters.

We now continue to evaluate the Wigner function for the singlet-doublet fields. For this purpose, we start from the normally ordered characteristic function $\chi_{\rm SD}$ in the singlet-doublet factorization. Especially, if we insert Eq. (64) into Eq. (38), we get

$$W_{\rm SD}(\alpha) = \frac{1}{\pi^2}\int d^2\eta e^{(\langle \hat{B}^\dagger\rangle - \alpha^\star)\eta - (\langle \hat{B}\rangle - \alpha)\eta^\star - [\Delta\langle \hat{B}^\dagger \hat{B}\rangle + (1/2)]\eta\eta^\star + (\Delta\langle \hat{B}\hat{B}\rangle/2)[\eta^\star]^2 + (\Delta\langle \hat{B}^\dagger \hat{B}^\dagger\rangle/2)\eta^2}. \tag{72}$$

This integral is fully convergent due to its Gaussian form. By applying the definitions (69) and (70), we eventually obtain

$$W_{\rm SD}(\alpha) = \frac{1}{2\pi\Delta X\Delta Y} e^{-1/2[(\Delta\alpha_1^2/\Delta X^2) + (\Delta\alpha_2^2/\Delta Y^2)]},$$

$$\Delta\alpha_1 \equiv (\alpha_1 - \beta_1)\cos\phi - (\alpha_2 - \beta_2)\sin\phi,$$

$$\Delta\alpha_2 \equiv (\alpha_1 - \beta_1)\sin\phi + (\alpha_2 - \beta_2)\cos\phi, \tag{73}$$

i.e., a Gaussian function whose width is determined by Eq. (70) while the angle ϕ follows from $e^{i2\phi} = \frac{\Delta\langle BB\rangle}{|\Delta\langle BB\rangle|}$. From Eq. (72), we conclude that the contour lines of the singlet-doublet Wigner function are determined by an ellipse that is centered at $(\alpha_1, \alpha_2) = (\beta_1, \beta_2)$ and whose main axes are rotated by the angle $-\phi$ with respect to the α_1 axis as shown in Fig. 4. The main axes of the ellipse are determined by ΔX and ΔY such that the Wigner function can have different extensions into the α_1 and α_2 directions. Since ΔX and ΔY are directly related to the maximum and minimum fluctuations of the quadratures corresponding to the momentum and position quadratures, the main axes of the ellipse present the physical extreme values of the quadrature fluctuations. At this point, we also observe that $W_{\rm SD}(\alpha)$ is fully positive such that quantum fields with negative values in some phase-space regions must follow from clusters beyond doublets.

D. From correlated clusters to the phase-space representation

The singlet-doublet example demonstrates that one gets a converging transformation from correlated clusters to the

phase-space representation for any physical Gaussian field, described by coherent-thermal-squeezed states, which is not generally possible when starting from the I_K^J representation alone. Even the description of the thermal state is convergent, despite the numerical instability for the I_K^J-to-W mapping identified in Sec. IV B. As a key element, the clusters represent the characteristic function with a finite number of terms instead of the possibly infinite I_K^J terms.

As a next step, we explore how well clusters describe fields with correlations of higher orders than doublets. It is rather easy to see that, e.g., the inclusion of triplets does not work if one applies the simplest implementation in the form $\chi_{\mathrm{SDT}}(\beta)=e^{\xi_{\mathrm{SDT}}(\beta)}$ in Eq. (38) because the cubic term does not yield converging integrals. Thus, we need to apply a more sophisticated approach to fully benefit from the convergence provided by the singlet-doublet contributions. For this purpose, we introduce a splitting between the singlet-doublet and the higher-order correlations via the cluster-expansion separation,

$$\chi_{\mathrm{N}}(\beta) \equiv e^{\xi_{\mathrm{SD}}(\beta)}A(\beta) = \chi_{\mathrm{SD}}(\beta)A(\beta),$$

$$A(\beta) = \frac{\chi_{\mathrm{N}}(\beta)}{\chi_{\mathrm{SD}}(\beta)} = \sum_{J,K=0}^{\infty} \frac{\beta^J[-\beta^\star]^K}{J!K!}a_K^J. \tag{74}$$

In this form, the singlet-doublet contributions are included via their correlation-generating function while all higher-order clusters are seprated and described with a Taylor expansion. Since $\chi_{\mathrm{SD}}(\beta)$ is a nonvanishing analytic function for all values of β, also $A(\beta)$ remains analytic and exists in the vicinity of $\beta=0$. Thus, the Taylor-expansion form can always be identified. At this point, we utilize this fact only formally and work out explicit expressions related to the coefficients a_K^J later.

If we perform the systematic truncation to the cluster $C \geqslant 2$, Eq. (74) becomes

$$\chi_{1\cdots C}(\beta) = e^{\xi_{\mathrm{SD}}(\beta)}A_C(\beta),$$

$$A_C(\beta) = \sum_{J,K=0}^{C} \frac{\beta^J[-\beta^\star]^K}{J!K!}a_K^J. \tag{75}$$

This systematic truncation describes all expectation values up to C particles exactly. Beyond these C-particle expectation values, all singlet-doublet factorizations and the dominant $(3\ldots C)$-particle correlations are included, whereas clusters beyond C are neglected. Obviously, this approximation can be systematically improved by increasing C. If we now insert Eq. (75) into Eq. (38), we find

$$W(\alpha) = \frac{1}{\pi^2}\int d^2\beta A_C(\beta) \times e^{-[\Delta\langle\hat{B}^\dagger B\rangle+(1/2)]|\beta|^2+(\Delta\langle\hat{B}^\dagger\hat{B}^\dagger\rangle/2)\beta^2+(\Delta\langle BB\rangle/2)(\beta^\star)^2} \times e^{\beta^\star(\alpha-\langle B\rangle)-\beta(\alpha^\star-\langle\hat{B}^\dagger\rangle)}, \tag{76}$$

after we express $\xi_{\mathrm{SD}}(\beta)$ with the help of Eq. (64). We now notice a large difference in comparison to Eq. (53): With the help of the cluster-expansion formulation, the transformation obtains an additional Gaussian convergence factor $\Delta\langle\hat{B}^\dagger\hat{B}\rangle$ that will make the approach (76) fully convergent for physical sources, as shown later in Sec. V.

The explicit evaluation of Eq. (76) is performed in Appendix B, where we introduce an auxiliary phase-space distribution and a correlation-generating function

$$\bar{W}(\alpha) \equiv 4\Delta X\Delta Y W([2\Delta X\alpha_1 + i2\Delta Y\alpha_2]e^{i\phi} + \langle B\rangle),$$

$$\bar{A}(\beta) \equiv A\left(\left[\frac{\beta_1}{2\Delta Y} + i\frac{\beta_2}{2\Delta X}\right]e^{i\phi}\right) = \sum_{J,K}\frac{(-1)^{J+K}}{J!K!}\bar{a}_K^J\beta^J[-\beta^\star]^K, \tag{77}$$

respectively, where ΔX and ΔY are defined by Eq. (70). As a general property, the cluster orders appearing in $\bar{A}$ and A are identical. Especially, the truncation to C clusters is performed in the same manner. With these ingredients, Eq. (76) can be reformulated into

$$\bar{W}_C(\alpha) = \frac{1}{\pi^2}\int d^2\beta\bar{A}_C(\beta)e^{-(1/2)|\beta|^2}e^{-\beta^\star\alpha+\beta\alpha^\star} = \sum_{J,K=0}^{C}\frac{(-1)^K}{J!K!}\bar{a}_K^J\frac{1}{\pi^2}\int d^2\beta\beta^J[-\beta^\star]^K e^{-\beta^\star\alpha+\beta\alpha^\star}, \tag{78}$$

as shown in Appendix B. We now recognize that this expression has exactly the same functional form as the direct transformation (53). Thus, *the separation of singlet-doublet clusters*, via Eq. (74), *simply corresponds to a geometric transformation* (77) where the Wigner function is suitably translated and then squeezed and stretched in the perpendicular quadrature directions.

At first glance, one might think that the old convergence problem still remains. However, $\bar{W}(\alpha)$ has the unusual properties

$$\int d^2\alpha\bar{W}(\alpha) = 1, \quad \int d^2\alpha\alpha\bar{W}(\alpha) = 0,$$

$$\int d^2\alpha|\alpha|^2\bar{W}(\alpha) = \frac{1}{2}, \quad \int d^2\alpha\alpha^2\bar{W}(\alpha) = 0, \tag{79}$$

that differ considerably from averages of generic Wigner functions. In fact, only a vacuum state $W(\alpha)$ has a phase-space distribution fulfilling all of the relations (79). Thus, $\bar{W}$ is not necessarily a phase-space distribution of a physical field, however it is a vacuumlike distribution with respect to its lowest momenta. Since the transformations (53) and (78) exhibit extreme convergence for the vacuum state, we may expect that the *vacuumlike properties* (79) *guarantee the convergence for the cluster-expansion form* (78). In other words, the geometric transformation (77) rescales the Wigner function to a format where it resembles the vacuum as much as possible, which produces a numerically stable mapping from expectation values to the Wigner function. In practice, the coefficients $\bar{a}_K^J$ can be computed from Eq. (42) if we make the simple identification $\bar{W}\leftrightarrow W$ and $\bar{a}_K^J\leftrightarrow I_K^J$.

Since experiments often access the marginal distributions rather than Wigner functions, we modify the cluster-expansion separation such that it can easily be applied to convert clusters into $P_\theta(x)$. For this purpose, we start from

$$\xi_N^\theta(iy) \equiv \xi_N(iye^{i\theta}) = \sum_{J,K=0}^{\infty} \frac{(iy)^{J+K}}{J!K!} \Delta I_K^J e^{i\theta(J-K)} = \sum_{L=0}^{\infty} (iy)^L \Delta I_{\Sigma,L}^\theta, \tag{80}$$

$$\Delta I_{\Sigma,L}^\theta \equiv \sum_{J=0}^{L} \frac{e^{i\theta(2J-L)}}{J!(L-J)!} \Delta I_{L-J}^J, \tag{81}$$

where the last step of Eq. (80) follows from the same kind of derivation as that performed in connection with Eq. (47). This procedure introduces a collective L-particle correlation $\Delta I_{\Sigma,L}^\theta$ in analog to Eq. (47). It is straightforward to show that each $\Delta I_{\Sigma,L}^\theta$ contains products of expectation values that together have exactly L photon operators. In particular, the singlet-doublet clusters can be defined via

$$\Delta I_{\Sigma,0}^\theta = 0, \quad \Delta I_{\Sigma,1}^\theta = I_{\Sigma,1}^\theta = \langle (2\hat{x}_\theta) \rangle \equiv 2X_\theta,$$

$$\Delta I_{\Sigma,2}^\theta = I_{\Sigma,2}^\theta - \frac{1}{2} I_{\Sigma,1}^\theta I_{\Sigma,1}^\theta = \frac{\langle (2\hat{x}_\theta)^2 \rangle - \langle (2\hat{x}_\theta) \rangle^2 - 1}{2} \equiv 2\Delta X_\theta^2 - \frac{1}{2}, \tag{82}$$

where we have also applied Eq. (34) to unravel the direct connection to the quadrature fluctuations. If we now evaluate Eq. (80) with singlet-doublet contributions only, the identification (82) produces Eq. (65) as derived earlier.

By applying the basic idea of the cluster-expansion separation, we next include the singlet $L=1$ and doublet $L=2$ correlations to all orders in the characteristic function while higher-order clusters are described with a Taylor expansion. This goal can be reached as we modify Eq. (80) by introducing the cluster-expansion separation,

$$\chi_N^\theta(iy) = e^{\xi_{\mathrm{SD}}^\theta(iy)} A_N^\theta(iy), \quad y \in \mathbb{R}$$

$$A_N^\theta(iy) \equiv \sum_{J=0}^{\infty} a_{\Sigma,J} (iy)^J, \quad \xi_{\mathrm{SD}}^\theta(iy) = 2iyX_\theta - 2y^2 \left(\Delta X_\theta^2 - \tfrac{1}{2} \right). \tag{83}$$

Here, we have applied Eqs. (65) and (80)–(82) and identified the collective Taylor-expansion coefficients $a_{\Sigma,J}$. If we now truncate this sum at the level of a C-particle cluster, the singlet-doublet correlations are included to all orders while the higher-order correlations are systematically truncated at the C-particle correlations.

As expression (83) is inserted back into Eq. (39), we now get

$$P_\theta(x) = \sum_{J=0}^{\infty} a_{\Sigma,J} \frac{1}{\pi} \int dq (iq)^J e^{2i(x-X_\theta)q - 2\Delta X_\theta^2 q^2}. \tag{84}$$

For the Wigner function, we find the geometric transformation

$$\bar{P}_\theta(x) = 2\Delta X_\theta P(2\Delta X_\theta x + X_\theta), \quad \bar{a}_{\Sigma,J} \equiv \frac{a_{\Sigma,J}}{[2\Delta X_\theta]^J} \tag{85}$$

for the singlet-doublet separation (83). With these results, we can simplify Eq. (84) into

$$\bar{P}_\theta(x) = \sum_{J=0}^{\infty} \bar{a}_{\Sigma,J} p^{(J)}(x). \tag{86}$$

We notice that this transformation has the same form as Eq. (55) when we identify $\bar{a}_{\Sigma,J}$ to correspond to $I_{\Sigma,J}$. Thus, the cluster-expansion separation is essentially a simple geometric transformation (85) where the probability distribution is displaced by X_θ while the x coordinate is additionally rescaled by the width of the distribution. Due to this exact analogy, the coefficients $\bar{a}_{\Sigma,J}$ can be evaluated from a known distribution function using Eq. (48) in a form where $I_{\Sigma,J}$ is replaced by $\bar{a}_{\Sigma,J}$ and P is replaced by $\bar{P}$, respectively.

The cluster-expansion separation introduces a major advantage in comparison to the direct transformation (55). The *rescaled distribution* has a form whose lowest moments are identical to that of the vacuum state, i.e.,

$$\int dx \bar{P}_\theta(x) = 1, \quad \int dx x \bar{P}_\theta(x) = 0, \quad \int dx x^2 \bar{P}_\theta(x) = \frac{1}{4}. \tag{87}$$

In other words, $\bar{P}_\theta(x)$ is a distribution that is centered at the origin with the quadrature fluctuations of the vacuum. Since the direct transformation close to the vacuum state shows extreme convergence, the cluster-expansion separation produces a converging transformation from expectation values and correlations into the phase-space representation.

E. Cluster-expansion transformation (CET)

We may now summarize the transformation between the cluster-expansion separation and the phase-space representation into a simple algorithm. First of all, we can drop the quadrature-index label since the same index appears in all terms. We then start from a generic marginal distribution $P(x)$ that produces the average and variance via

$$X = \int dx x P(x), \quad \Delta X^2 \equiv \int dx x^2 P(x) - X^2. \tag{88}$$

The obtained X and ΔX introduce the geometric transformation

$$\bar{P}(x) = 2\Delta X P(2\Delta X x + X) \tag{89}$$

to the rescaled distribution according to Eq. (85). This is the central relation following from the separation of singlet-doublet contributions from the higher-order clusters. The obtained $\bar{P}(x)$ defines then the moments and the $\bar{a}_{\Sigma,J}$ correlations,

$$\langle (2\bar{x})^j \rangle \equiv \int_{-\infty}^{\infty} dx \frac{(2x)^j}{j!} \bar{P}(x), \quad \bar{a}_{\Sigma,L} = \sum_{K=0}^{[L/2]} \frac{\langle (2\bar{x})^{L-2K} \rangle}{(-2)^K K!}, \tag{90}$$

where we have used Eqs. (48) and (86). The inverse transformation follows from

$$\bar{P}(x) = \sum_{J=0}^{\infty} \bar{a}_{\Sigma,J} p^{(J)}(x),$$

$$p^{(K)}(x) = \frac{1}{\sqrt{2\pi}} e^{-(1/2)x^2} \sum_{J=0}^{[K/2]} \frac{K!}{J!(K-2J)!} \frac{x^{K-2J}}{(-2)^J}, \tag{91}$$

where we have combined Eqs. (56) and (86). This can now be converted back to the form of the original distribution by applying

$$P(x) = \frac{1}{2\Delta X} \bar{P}\left(\frac{x - X}{2\Delta X} \right), \tag{92}$$

which completes the cycle from probability distribution to correlated clusters and back. The steps (88)–(92) constitute the cluster-expansion transformation (CET). It can be performed for all relevant quadrature directions allowing us to construct the Wigner function from clusters by applying the Radon transformation (37) after step (92).

To have a practical scheme to test the convergence of the transformation (91), we investigate how fast the corresponding sum approaches the original input distribution when only a finite number of clusters C is included. Since $\bar{P}(x)$ is centered at $x=0$, it is natural to follow $\bar{P}(x)$ at its central value,

$$\bar{P}(0) = \sqrt{\frac{2}{\pi}} \sum_{J=0}^{C} \bar{\bar{a}}_{\Sigma,2J}, \quad \bar{\bar{a}}_{\Sigma,2J} \equiv \frac{(2J)! \bar{a}_{\Sigma,2J}}{(-2)^J J!},$$

$$\left. \frac{d\bar{P}(x)}{dx} \right|_{x=0} = 2\sqrt{\frac{2}{\pi}} \sum_{J=0}^{C} \bar{\bar{a}}_{\Sigma,2J+1},$$

$$\bar{\bar{a}}_{\Sigma,2J+1} \equiv \frac{(2J+1)! \bar{a}_{\Sigma,2J+1}}{(-2)^J J!}, \tag{93}$$

where we used Eq. (91). It is interesting to notice that only even coefficients $\bar{\bar{a}}_{\Sigma,2J}$ contribute to $\bar{P}(x=0)$ while only the odd coefficients appear in its derivative. Additionally, we have evaluated $p^{(J)}(x=0)$ using Eq. (56) to obtain the prefactors. We combine these factors into $\bar{\bar{a}}_J$, which is the quantity of interest for the convergence analysis. The convergence of the cluster-expansion approach requires that $\bar{\bar{a}}_{\Sigma,J}$ forms a series that decays faster than $1/J$ for large enough J. Even though convergence at one point formally does not guarantee the most general convergence at an arbitrary x, the reference point at $x=0$ has a special significance: (i) the form of the distribution $\bar{P}(x=0)$ in the vicinity of the center is definitely the most decisive region to determine the quantum statistics, and (ii) the $p^{(J)}(x)$ functions in Eq. (91) have a Gaussian decay away from $x=0$. Thus, convergence at $x=0$ must be an extremely sensitive indicator whether Eq. (91) is capable of converging everywhere. We will show numerically that Eq. (93) indeed quantifies the general convergence properties.

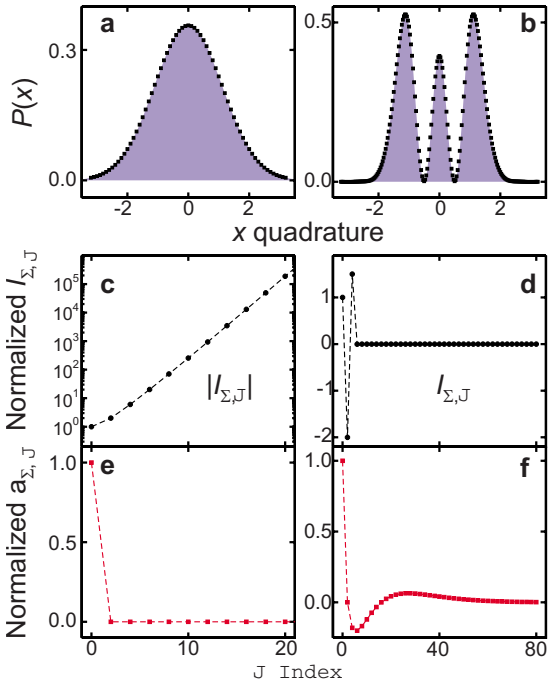

FIG. 5. (Color online) Convergence of normalized expectation value and correlation quantities in the quantum-state reconstruction. (a) A marginal distribution of the two-photon thermal state (shaded area) is shown together with the cluster-expansion reconstruction (filled squares). The CET has $C=20$ terms. The corresponding $\bar{\bar{I}}_{\Sigma,J}$ and $\bar{\bar{a}}_{\Sigma,J}$ are shown in (c) and (e), respectively. (The dashed line is a guide to the eye.) The same quantities are presented in (b), (d), and (f) for the Fock state $|2\rangle$. Here, the CET has $C=80$ terms.

The same convergence analysis can be repeated for the direct expectation-value conversion (55). Here, we find the normalized collective expectation values

$$\bar{\bar{I}}_{\Sigma,2J} \equiv \frac{(2J)!}{(-2)^J J!} I_{\Sigma,2J},$$

$$\bar{\bar{I}}_{\Sigma,2J+1} \equiv \frac{(2J+1)!}{(-2)^J J!} I_{\Sigma,2J+1}. \tag{94}$$

This result is very similar to Eq. (93) due to the close analogy provided by the cluster-expansion separation. The expectation-value representation can be converted into the phase space in a numerically feasible manner whenever $\bar{\bar{I}}_{\Sigma,J}$ produces a series that decays faster than $\frac{1}{J}$.

To investigate the convergence of the cluster-expansion implementation, we have evaluated both $\bar{\bar{I}}_{\Sigma,J}$ and $\bar{\bar{a}}_{\Sigma,J}$ for a Fock state $|2\rangle$ and a thermal state with $n_{\mathrm{th}}=2$ photons on average. More specifically, we use the distributions (49) and (51) as an input and then perform the CET (88)–(92). In the process, we obtain $\bar{\bar{I}}_{\Sigma,J}$ and $\bar{\bar{a}}_{\Sigma,J}$ as well as the distribution constructed explicitly via the cluster expansion. Figure 5 presents the original input distributions (shaded area) as well as the CET results (squares) for (a) the thermal state and (b) the

Fock state $|2\rangle$. The corresponding normalized $\bar{\bar{I}}_{\Sigma,J}$ are shown in Figs. 5(c) and 5(d) while the cluster-expansion coefficients are plotted in Figs. 5(e) and 5(f).

In contrast to the direct-transformation results of Fig. 4, the cluster-expansion transformation fully reproduces the original input distribution in a numerically feasible manner even for the thermal state with $n_{\mathrm{th}} \geqslant \frac{1}{2}$. In fact, one needs only clusters up to doublets ($C=2$) for any value of n_{th}. The same level of accuracy is obtained for any coherent or squeezed state distribution defined by Eqs. (50) and (52), respectively. For the Fock state, $C=80$ clusters reproduce $P(x)$ with extreme accuracy. The minimum number of actually needed C is studied later in Sec. V.

The collective expectation values and correlations are evaluated using the CET and Eqs. (92)–(94). The results are shown in the middle frames of Fig. 5 for $\bar{\bar{I}}_{\Sigma,J}$ and the lowest frames for $\bar{\bar{a}}_{\Sigma,J}$, respectively. As in Fig. 2, $\bar{\bar{I}}_{\Sigma,J}$ diverges rapidly for the thermal state, which implies a diverging numerical transformation from expectation values to marginal distributions. However, the corresponding correlations produce a series that converges so well that $\bar{\bar{a}}_{\Sigma,J=0}$ is the only nonvanishing term. An identical $\bar{\bar{a}}_{\Sigma,J}$ series is found for any Gaussian field because the cluster-expansion separation, especially Eq. (90), transforms the distribution to the same vacuum distribution. As observed before in Sec. IV D, this transformation produces extreme convergence for the $\bar{\bar{a}}_{\Sigma,J}$ series and its conversion into a marginal distribution, Eq. (92).

At the same time, the Fock state displays a $\bar{\bar{I}}_{\Sigma,J}$ that first seems to diverge. As before, we observe an abrupt convergence in $\bar{\bar{I}}_{\Sigma,J}$ as J is increased above $J=4$ (note that both $\bar{\bar{a}}_{\Sigma,J}$ and $\bar{\bar{I}}_{\Sigma,J}$ vanish for odd J). Thus, the expectation values can be converted into marginal distributions of a Fock state such that one does not necessarily need the clusters in the numerical analysis. When the cluster-expansion implementation is applied for the Fock state, we find that $\bar{\bar{a}}_{\Sigma,J}$ remains small and converges smoothly toward $\bar{\bar{a}}_{\Sigma,J}=0$ for large enough J. This result indicates that we may indeed truncate the sum (92) into a finite number of terms and still expect an excellent representation of the distribution. As discussed above, $C=80$ clusters produce $|2\rangle$ accurately. The relatively large number of needed clusters indicates that a Fock state is a true quantum field with a high degree of correlations.

These examples illustrate several general aspects of the cluster-expansion transformation. Especially, $\bar{\bar{a}}_{\Sigma,J}$ forms a converging series even when $\bar{\bar{I}}_{\Sigma,J}$ is diverging. We show later, in Sec. V A, that this observation holds for generic physical distributions. As a result, we may truncate the expansion into a finite number of terms, which directly implies that the infinite-dimensional quantum statistics can accurately be represented by a finite number of correlations. This property makes the cluster expansion an attractive scheme to describe quantum-optical fields. For the important quantum-statistical subgroup of coherent-thermal-squeezed states, one only needs the singlet-doublet clusters for the high-quality, numerically stable description of the light.

Generally, these observations do not yet define how large J must be for a given source. Thus, it is often beneficial to analyze how both $\bar{\bar{I}}_{\Sigma,J}$ and $\bar{\bar{a}}_{\Sigma,J}$ behave as a function of J. In the case in which $\bar{\bar{I}}_{\Sigma,J}$ drops to very low values after some threshold J, we may want to use the direct implementation while the cluster-expansion transformation is the only viable solution when $\bar{\bar{I}}_{\Sigma,J}$ diverges.

V. CONVERGENCE OF CLUSTER EXPANSION

Based on the results in Sec. IV D, the cluster expansion provides a useful transformation to convert expectation value and correlation representations into the phase-space representation. Since the Wigner function can always be reconstructed topographically whenever we know the relevant marginal distributions, we investigate next how the mapping of the cluster expansion into phase-space representations—and vice versa—generally converges for any physically relevant marginal distribution. Since P_θ and W are connected via the Radon transformation (37), this analysis tells us directly how the cluster-expansion approach and the phase-space representation are connected in practice.

We investigate the convergence of the cluster expansion by performing the full CET cycle (88)–(92) with an arbitrary $P(x)$ as an input. To isolate different convergence aspects, it is convenient to use a subdivision

$$P(x) = \sum_{\lambda} P_\lambda(x), \quad \bar{P}(x) = \sum_{\lambda} \bar{P}_\lambda(x) \tag{95}$$

of the probability distribution into different components labeled by λ. This subdivision can, e.g., represent a decomposition into different functional bases or the division of $P(x)$ into intervals. We notice that the CET Eqs. (88)–(91) provide a linear transformation. In other words, each component $\bar{P}_\lambda(x)$ produces its own cluster-expansion coefficients giving independent $\bar{a}^{\lambda}_{\Sigma,J}$ correlations for each $\bar{P}_\lambda$. If we now apply $\bar{\bar{a}}^{\lambda}_{\Sigma,J}$ to transform back to the phase-space picture, the linear sum of resulting functions is then the original probability distribution. By analyzing the convergence of the cluster expansion against the corresponding $\bar{P}_\lambda(x)$, we can conclude which of the isolated parts converges.

A. Cluster expansion for central parts of distributions

If one considers physically relevant marginal distributions, they clearly have to be analytic functions. Furthermore, they decay toward zero sufficiently far away from their central peak value. Especially, if P is a measured quantity, it is bound to approach zero outside a given region of interest. Thus, the rescaled $\bar{P}(x)$ decays rapidly beyond its half-width value, i.e., $|x| \gg \frac{1}{2}$, for all physically relevant probability distributions.

To analyze the convergence related to the central parts of any given distribution, we subdivide an arbitrary $\bar{P}(x)$ into separate parts using a boxlike function

$$T_{\bar{\epsilon}}(x,\bar{R}) = E_{\bar{\epsilon}}(x+\bar{R}) - E_{\bar{\epsilon}}(x-\bar{R}),$$

$$E_{\bar{\epsilon}}(x) = \frac{1}{\sqrt{\pi\bar{\epsilon}^2}} \int_{-\infty}^{x} dy e^{-y^2/\bar{\epsilon}^2}, \tag{96}$$

where the error function $E_{\bar{\epsilon}}(x)$ provides a smooth step at $x=0$ while the steepness of the step is controlled by $\bar{\epsilon}$. Note that both $\bar{R}$ and $\bar{\epsilon}$ are presented in scaled units that are provided by the geometric transformation (89). The central and tail parts of any given distribution can be extracted by introducing

$$\bar{P}(x) = \bar{P}_{\text{cent}}(x) + \bar{P}_{\text{tail}}(x),$$

$$\bar{P}_{\text{cent}}(x) = T_{\bar{\epsilon}}(x,\bar{R})\bar{P}(x),$$

$$\bar{P}_{\text{tail}}(x) = [1 - T_{\bar{\epsilon}}(x,\bar{R})]\bar{P}(x). \tag{97}$$

When $\bar{R}$ is chosen large enough, $\bar{P}_{\text{cent}}(x)$ always contains the experimentally accessible parts of the distribution while $\bar{P}_{\text{tail}}(x)$ contains only the physically insignificant tails.

Using this subdivision, we next study what kind of general convergence follows from the central part alone. We may conclude from Eq. (93) that the convergence of the cluster-expansion approach depends critically on how the $\bar{a}^{\text{cent}}_{\Sigma,J}$ coefficients behave for large values of J. Thus, we investigate how these coefficients, which are related to $\bar{P}_{\text{cent}}(x)$, converge asymptotically. We start from Eq. (90) giving

$$\langle(2\bar{x})^{2j}\rangle_{\text{cent}} \equiv \int_{-\infty}^{\infty} dx \frac{(2x)^{2j}}{(2j)!}\bar{P}_{\text{cent}}(x) = \int_{0}^{\infty} dx \frac{(2x)^{2j}}{(2j)!} T_{\bar{\epsilon}}(x,\bar{R}) \times [\bar{P}(x) + \bar{P}(-x)], \tag{98}$$

which follows since $(2x)^{2j}$ and $T_{\bar{\epsilon}}(x,\bar{R})$ are symmetric functions. If we consider the case with $\bar{\epsilon}=0$, we realize that $T_{\bar{\epsilon}}(x,\bar{R})$ is a step function whose value is 1 for $|x| \leqslant R$ while it vanishes everywhere else. For this situation, the integrand in Eq. (98) is strongly peaked close to $x=\pm\bar{R}$ when j is large enough. In other words, the integrand $\frac{(2x)^{2j}}{(2j)!}T_{\bar{\epsilon}}(x,\bar{R})$ behaves much like two δ functions located at the borders of the integration interval. This property also holds for not too large values of $\bar{\epsilon}$ since $\bar{\epsilon}>0$ just implies a smooth step. By making use of this observation, we may evaluate Eq. (98) through

$$\langle(2\bar{x})^{2j}\rangle_{\text{cent}} \equiv \int_{-\infty}^{\infty} dx \frac{(2x)^{2j}}{(2j)!}\bar{P}_{\text{cent}}(x) = \int_{0}^{\infty} dx \frac{(2x)^{2j}}{(2j)!} T_{\bar{\epsilon}}(x,\bar{R}) \times [\bar{P}_{\text{cent}}(x) + \bar{P}_{\text{cent}}(-x)] = 2\bar{P}^{E}_{\text{cent}}(\bar{R}) \int_{0}^{\infty} dx \frac{(2x)^{2j}}{(2j)!} T_{\bar{\epsilon}}(x,\bar{R}), \quad j \gg 1, \tag{99}$$

where we have identified the even part of the function $\bar{P}_{\text{cent}}(x)$ via $\bar{P}^{E}_{\text{cent}}(x) \equiv \frac{\bar{P}_{\text{cent}}(x)+\bar{P}_{\text{cent}}(-x)}{2}$. The resulting expression (99) is accurate as long as j is large enough, the $\bar{P}_{\text{cent}}(\pm\bar{R})$ are nonvanishing, and they represent $\bar{P}_{\text{cent}}(x)$ well in the vicinity of $x=\pm\bar{R}$. The remaining integral can be evaluated analytically giving

$$\langle(2\bar{x})^{2j}\rangle_{\text{cent}} = \bar{P}^{E}_{\text{cent}}(\bar{R}) \sum_{k=0}^{j} \frac{(2\bar{R})^{2k+1}\bar{\epsilon}^{2(j-k)}}{(2k+1)!(j-k)!}, \quad j \gg 1. \tag{100}$$

In general, $\bar{a}^{\text{cent}}_{\Sigma,2L}$ for large L is dominated by $\langle(2\bar{x})^{2j}\rangle$ at large values of j. Thus, the convergence of any particular cluster expansion can be studied by applying the large j-value limit of Eq. (100) for all j. In other words, Eq. (100) isolates that contribution which is critical for the convergence. This contribution can then be inserted into Eqs. (90) and (93), giving the convergence-critical contributions

$$\bar{a}^{\text{conv}}_{\Sigma,2L} = 2\bar{R}\bar{P}^{E}_{\text{cent}}(\bar{R}) \sum_{J=0}^{L} \frac{(2\bar{R})^{J}}{(2J+1)!(L-J)!} \left(\bar{\epsilon}^2 - \frac{1}{2}\right)^{L-J}. \tag{101}$$

We notice that the choice $\bar{\epsilon}^2=\frac{1}{2}$ simplifies the result into the single term $J=L$, yielding

$$\bar{a}^{\text{conv}}_{\Sigma,2L} = \bar{P}^{E}_{\text{cent}}(\bar{R}) \frac{(2\bar{R})^{2L+1}}{(2L+1)!},$$

$$\bar{a}^{\text{conv}}_{\Sigma,2L+1} = 2\bar{P}^{E}_{\text{cent}}(\bar{R}) \frac{(-2)^{L}}{L!} \frac{\bar{R}^{2L+1}}{(2L+1)!}, \tag{102}$$

where $\bar{a}^{\text{conv}}_{\Sigma,2L}$ follows from the definition (93). Hence, the potentially diverging terms in the cluster expansion actually produce a convergent series

$$\bar{P}^{\text{conv}}_{\text{cent}}(0) = \sqrt{\frac{2}{\pi}} 2\bar{P}^{E}_{\text{cent}}(\bar{R}) \sum_{L=0}^{\infty} \frac{(-2)^{L}}{L!} \frac{R^{2L+1}}{(2L+1)} = \bar{P}^{E}_{\text{cent}}(\bar{R}) T_{\bar{\epsilon}=1/\sqrt{2}}(x=0,\bar{R}), \tag{103}$$

where Eq. (102) has been inserted into Eq. (93). This result has an interesting interpretation: The cluster expansion of an arbitrary probability distribution always converges as far as its central parts are concerned. The convergence of the cluster-expansion approach, therefore, only depends on the tail parts of the distribution. The truncated tails contribute to the central value with a weight that is the average of the distribution at the borders. Since the remaining tail parts can be made vanishingly small for physically relevant sources, we do not need to even consider what happens to these physically insignificant contributions. Thus, we have shown that *the CET always converges for physical distributions because it automatically accesses the physically important parts of the distribution while the physically insignificant parts, with apossible divergent behavior, are filtered out*.

Even though the sum in Eq. (103) is convergent, we have not yet determined how many clusters are needed to produce an accurate CET. If we limit the L sum to the C-particle cluster, the highest index of summation in Eq. (103) is $[\frac{C}{2}]$. Since the first omitted sum term determines the level of error in truncation for converging sums, we get an error estimate

$$\Delta\epsilon^{C}_{\text{cent}} \equiv \bar{\bar{a}}_{\Sigma,2[(C/2)+1]} = \sqrt{\frac{2}{\pi}}\bar{P}^{\text{even}}_{\text{cent}}(\bar{R}) \times (-1)^{(C/2)+1}\frac{(-2\bar{R}^2)^{(C/2)+1}}{[(C/2)+1]!}\frac{\bar{R}}{C+3} \tag{104}$$

for the truncation to C-particle clusters; note that C is assumed to be even. By using the relation

$$\frac{N^J}{J!}e^{-N} = \frac{1}{\sqrt{2\pi N}}e^{-(J-N)^2/2N} \quad \text{for large } J, \tag{105}$$

we can rewrite the error in the form

$$\Delta\epsilon^{C}_{\text{cent}} = \bar{P}^{\text{even}}_{\text{cent}}(\bar{R})\frac{(-1)^{(C/2)+1}}{\sqrt{2}\pi}\frac{1}{C+3}e^{-[(C+2)^2-8(C+2)\bar{R}^2-16\bar{R}^4]/16\bar{R}^2}. \tag{106}$$

It is now straightforward to show that the appearing exponential function is maximized at $C=4\bar{R}^2-2$ giving

$$\Delta\epsilon^{4\bar{R}^2}_{\text{cent}} = \frac{1}{\sqrt{2}\pi}\frac{1}{4\bar{R}^2+1}e^{+2\bar{R}^2}\bar{P}^{\text{even}}_{\text{cent}}(\bar{R}). \tag{107}$$

We notice that for a small number of terms, the error becomes large if $\bar{P}^{\text{even}}_{\text{cent}}(\bar{R})$ decays slower than $e^{-2\bar{R}^2}$. Thus, slowly decaying probability distributions can show a slow convergence even when truncated. However, as the cluster number grows beyond the limit

$$C \geqslant 4\bar{R}^2(1+\sqrt{2}) \approx 10\bar{R}^2, \tag{108}$$

the cluster expansion produces very convergent results. We can therefore use this relation to estimate the needed cluster number to reproduce the region of interest specified for the scaled distribution.

Most of the physically relevant marginal distributions have a Gaussian decay such that the investigated tail-related convergence problems do not appear. To get insight into how tails contribute in a worst-case scenario, we consider a Lorentzian marginal distribution,

$$P_{\text{Lor}}(x) = \frac{1}{\pi}\frac{1}{1+x^2}. \tag{109}$$

This distribution yields a diverging $\langle x^2\rangle$, which also implies an infinite photon number and energy within the field. Thus, $P_{\text{Lor}}(x)$ is not a possible distribution for physical fields. Nonetheless, if we now truncate $P_{\text{Lor}}(x)$ sharply at R and renormalize it, the rescaled distribution is limited within

$$\bar{R}_{\text{Lor}} \equiv \frac{R}{2\Delta X} = \frac{1}{2}\sqrt{\frac{R}{\arctan R}}. \tag{110}$$

We notice that $\bar{R}$ increases without a bound as R is elevated, which makes $P_{\text{Lor}}(x)$ an ideal distribution to explore how tails contribute to the CET.

Figure 6 presents the Lorentzian input distribution as a light (yellow) shaded area for three representative R: (a)-(c) $R=3$ ($\bar{R}_{\text{Lor}}=0.775$), (d)-(f) $R=6$ ($\bar{R}_{\text{Lor}}=1.033$), and (g)-(i) $R=12$ ($\bar{R}_{\text{Lor}}=1.42$), where the normalized truncation limits are

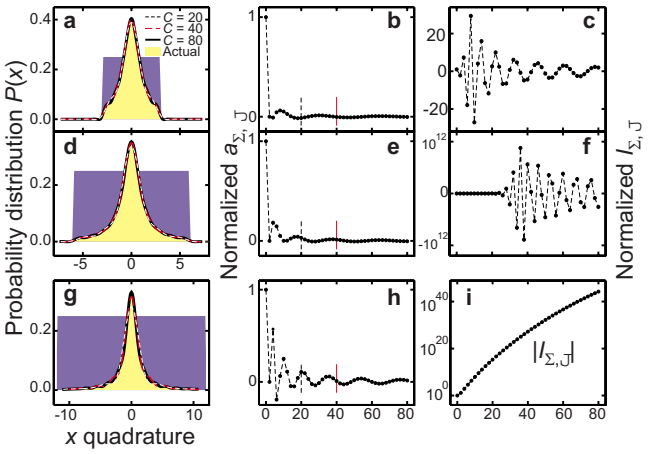

FIG. 6. (Color online) Convergence of cluster-expansion transformation for Lorentzian distributions. (a) The input $P(x)$, shown as the light (yellow) shaded area, is sharply truncated at $R=3$ indicated by the dark (blue) shaded area. The CET result with $C=20$ is shown as a white dashed line, for $C=40$ as (red) a dashed line, and for $C=80$ as a black line. (b) The corresponding $\bar{\bar{a}}_{\Sigma,J}$ correlations and (c) $\bar{\bar{a}}_{\Sigma,J}$ are plotted as filled circles. The dashed line is a guide to the eye. The same results are presented for the Lorentzian distributions, cut at $R=6$ (c)–(e) and at $R=12$ (f)–(i).

given in the parentheses. We have used a sharp truncation $\bar{\epsilon}$ for the sake of simplicity. The dark (blue) shaded rectangle indicates the position of the sharp truncation, i.e., the corresponding $T_{\bar{\epsilon}=0}(x)$ function. We have then applied the cluster-expansion transformation (88)–(92) and reproduced the distributions with $C=20$ clusters (white dashed line), $C=40$ clusters (red dashed line), and $C=80$ clusters (black line).

We note that the cluster expansion generally reproduces the distribution with a relatively small number of clusters. As a general trend, we need more clusters for elevated R in agreement with Eq. (108). In particular, the largest $R=12$ starts to show some oscillations when only a low number of clusters is included in the transformation. As C is increased, the oscillations become smaller and a clearly converging trend is observed even for the largest R used. As a visual estimate, Fig. 6 displays converging CET results for $C=20$, 40, and 80 for $\bar{R}=0.775$, 1.033, and 1.42, respectively. If a smooth truncation with $\bar{\epsilon}=\frac{1}{\sqrt{2}}$ were used, $C>6$, $C>11$, and $C>21$ should produce an accurate CET for $\bar{R}=0.775$, 1.033, and 1.42, respectively, according to Eq. (108). We have verified (not shown) that Eq. (108) accurately predicts the needed C-cluster number when a smooth truncation with $\bar{\epsilon}=\frac{1}{\sqrt{2}}$ is applied. Thus, as to be expected, a sharp truncation of tails produces a weaker convergence than a smooth truncation. An even better convergence can be reached by elevating $\bar{\epsilon}$ to $\frac{1}{2}$. In general, $\bar{\epsilon}$ can be used as a parameter to search for the best possible truncation of unphysical tails. Once the optimum $\bar{\epsilon}$ is found, the limit given in Eq. (108) can be considered as an upper cluster number that guarantees convergence for a suitably chosen $\bar{\epsilon}$.

To see the convergence of the cluster-expansion transformation directly, we have also evaluated the corresponding $\bar{\bar{a}}_{\Sigma,J}$ as well as $\bar{\bar{I}}_{\Sigma,J}$; see the middle and right-hand column of

Fig. 6. As for the previously studied physical distributions, $\bar{\bar{a}}_{\Sigma,J}$ forms a converging series. We also see that the convergence limits of C, discussed above, match very well with the regimes when $\bar{\bar{a}}_{\Sigma,J}$ becomes small. As a general trend, the oscillations in $\bar{\bar{a}}_{\Sigma,J}$ increase for elevated R. Especially, the long-living oscillations for $R=12$ can be associated with the elongated tails of the distribution. At the same time, $\bar{\bar{a}}_{\Sigma,J}$ either diverges or shows a poor convergence.

B. Cluster expansion for narrow features

Even though we have shown that the cluster expansion yields an accurate description for the physically relevant parts of the distribution, we do not yet know how accurately possible fine features within the region of interest are reproduced. To study this, we investigate how a narrow feature

$$\bar{P}_{\bar{F}}(x) = \bar{P}_0 e^{-2(x^2/\bar{F}^2)}, \quad 0 < \bar{F} < 1, \tag{111}$$

is reproduced by the CET. We assume here that the original distribution, $\bar{P}(x)=\bar{P}_{\bar{F}}(x)+\bar{P}_S(x)$, can be decomposed into parts including the investigated narrow feature and the remaining smooth distribution $\bar{P}_S(x)$. It is natural to assume that the feature has a narrower width than the average width of the overall distribution (i.e., $F<1$). Otherwise, it just contributes to the tails, i.e., the scenario investigated already in Sec. V A.

Based on the general additivity of the different components in probability distributions (see discussion in Sec. V), the convergence properties of the $\bar{P}_{\bar{F}}(x)$ part can be investigated independent of the other parts. In principle, this narrow feature can be shifted away from the origin, however this does not essentially change the investigation because trivial displacements do not change the efficiency of the cluster-expansion approach. Thus, for the sake of simplicity, we assume that the feature is centralized at the origin.

When we start from a given $\bar{P}_{\bar{F}}(x)$, we compute $\langle[2\bar{x}]^{2J}\rangle$ and convert it to $\bar{\bar{a}}^{F}_{\Sigma,2L}$ following the steps performed in Sec. V A. This procedure yields the normalized cluster-expansion coefficient,

$$\bar{\bar{a}}^{F}_{\Sigma,2L} = \bar{P}_0 \sqrt{\frac{\pi\bar{F}}{2}} \frac{(2L)!}{4^L L! L!} (1-\bar{F}^2)^L, \tag{112}$$

which yields a converging cluster-expansion series

$$\bar{P}_{\bar{F}}(0) = \sqrt{\frac{2}{\pi}} \sum_{J=0}^{\infty} \bar{\bar{a}}^{F}_{\Sigma,2J} = \bar{P}_0, \tag{113}$$

where Eq. (93) is applied. Here, the narrowness of the feature ($\bar{F}<1$) guarantees the convergence, in particular to the correct peak value of the feature. This result has also broader implications. Since we can isolate a narrow part anywhere within the distribution and reproduce its central value accurately, it is obvious that any narrow feature, and the probability distribution itself, can be reproduced with the cluster-expansion approach.

To see how rapidly the cluster expansion approaches its limiting value, we can analyze Eq. (113), which is truncated at the cluster C, i.e., the upper limit of J sum is set to $\frac{C}{2}$. Since the first omitted term yields an estimate for the error, we find that the cluster expansion has a relative accuracy of

$$\Delta\epsilon^F_C \equiv \frac{\bar{\bar{a}}^{F}_{\Sigma,C+2}}{\bar{P}_0} = \sqrt{\frac{\pi\bar{F}}{2}} \frac{(C+2)!}{2^{C+2}\left(\frac{C+1}{2}\right)!\left(\frac{C+1}{2}\right)!} (1-\bar{F}^2)^{C+1}. \tag{114}$$

We are particularly interested in cases in which the narrow feature is significantly smaller than the overall width of the entire distribution ($F \ll 1$). If we consider cases in which $\bar{F} < \frac{1}{3}$, we may approximate $(1-\bar{F}^2)^{C+1}$ by $e^{-\bar{F}^2(C+1)}$. Then, the functional form of Eq. (114) suggests that one needs a relatively large number of clusters to make ϵ^F_C small. Thus, we apply the large-C limit

$$\frac{(2C)!}{2^{2C}C!C!} = \frac{1}{\sqrt{\pi C}} \quad \text{for } C \gg 1 \tag{115}$$

to simplify the error estimate into

$$\Delta\epsilon^F_C = \sqrt{\frac{\bar{F}}{(C+1)}} e^{-\bar{F}^2(C+1)} \leqslant \frac{1}{8} e^{-\bar{F}^2 C}, \tag{116}$$

where we have assumed $F \leqslant \frac{1}{3}$ and $C \geqslant 22$. For these cases, we find a better than 1% accuracy whenever

$$C > \frac{2.5}{\bar{F}^2} \quad \text{for } \bar{F} \leqslant \frac{1}{3}. \tag{117}$$

At the limit of $F=\frac{1}{3}$, we find the limit $C>22.5$ such that all of our above assumptions are valid.

To see how the condition (114) can be applied in practice, we consider the cluster-expansion representation of different Fock states. The corresponding probability distributions $P_n(x)$ are defined by Eq. (49). In general, $P_n(x)$ has $n+1$ peaks where the furthermost peaks are close to $x=\pm\sqrt{n}$. The $n-1$ peaks within these extremes are spaced roughly equidistantly, separated by $\Delta r=\frac{2}{\sqrt{n}}$. The different peaks are well isolated since their width can be estimated by

$$\Delta x_n = \frac{\Delta r}{4} \sqrt{\frac{n}{n+1}} = \frac{1}{2\sqrt{n+1}}, \tag{118}$$

showing that the separation of two consecutive peaks is roughly $4\Delta x_n$. If we now approximate each peak with a Gaussian of the width Δx_n,

$$P^F_n(x) = \frac{0.64}{\sqrt{n+1}} e^{-4(n+1)x^2}, \quad n \geqslant 1, \tag{119}$$

gives a good approximation for the narrowest feature. Figure 7 presents several different Fock states (solid lines) together with the approximation $P^F_n(x)$ (shaded area) for the narrow feature. We see that the approximation reproduces the narrow feature very well.

The overall width of the Fock state is given by $\Delta X = \frac{1}{2}\sqrt{1+2\langle\hat{B}^\dagger B\rangle} = \frac{1}{2}\sqrt{1+2n}$. At the same time, the average of the quadratures vanishes for any given Fock state ($X=0$).

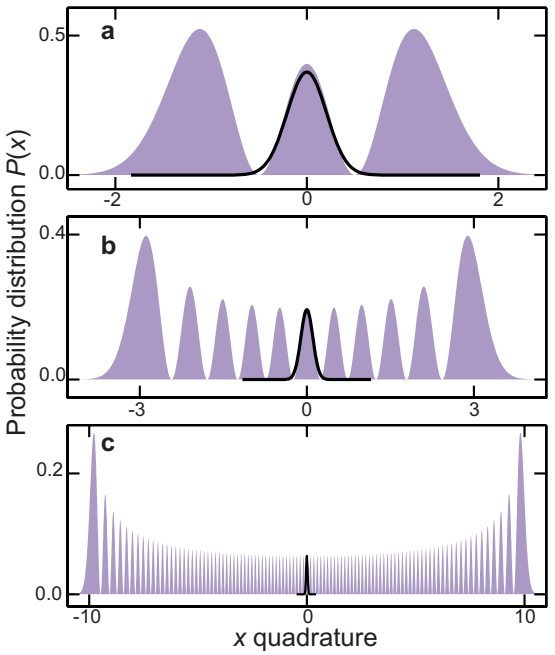

FIG. 7. (Color online) Probability distributions $P(x)$ for different Fock states. The overall $P(x)$ (shaded area) is compared with the result of Eq. (119) including only one narrow feature (solid line). The Fock states (a) $|2\rangle$, (b) $|10\rangle$, and (c) $|100\rangle$ are shown. The probability distributions follow from Eq. (49).

Combining these results with Eqs. (89) and (119), we find

$$\bar{P}_n^F(x) \equiv 2\Delta X P_n^F(2\Delta X x) = 0.64\sqrt{\frac{1+2n}{1+n}}e^{-2(x^2/\bar{F}_n^2)},$$

$$\bar{F}_n^2 = \frac{1}{2(1+n)(1+2n)}, \tag{120}$$

where $\bar{F}_n$ defines the ratio of the narrowest feature and the overall width for the Fock state $|n\rangle$. With the help of Eq. (117), we can estimate the number of clusters needed to describe a given feature. Using Eq. (120), we find that the peaks within the Fock state $|n\rangle$ are correctly reproduced whenever the upper cluster number satisfies

$$C > 5(1+n)(1+2n), \quad n \geqslant 1. \tag{121}$$

This estimate predicts that an accurate CET of Fock state $|1\rangle$ requires $C>30$, $|2\rangle$ with $C>75$, $|3\rangle$ with $C>140$, and $|4\rangle$ with $C>225$ clusters. Thus, the quantum-statistical complexity of the Fock states increases the number of clusters needed in the cluster-expansion representation.

C. General convergence criteria for the cluster expansion

The results in Secs. V A and V B determine clear and simple guidelines for judging how many clusters are needed to accurately describe a given quantum-statistical distribution. In a practical application, we first identify the central value of the distribution $X \equiv \int dx x P(x)$ and define its fluctuations $\Delta X^2 \equiv \int dx x P(x) - X^2$. We then determine the region of interest $|x-X| \leqslant \Delta R$ where all the physically relevant features of the distributions are located. Furthermore, we need to know the width ΔF of the narrowest feature, $P_{\text{feat}}(x) \propto e^{-2[(x-x_0)^2/\Delta F]}$, centered at x_0. As we apply the CET, the geometric transformation (89) determines the normalized widths

$$\bar{R} = \frac{\Delta R}{2\Delta X}, \quad \bar{F} = \frac{\Delta F}{2\Delta X}. \tag{122}$$

By combining these results with Eqs. (108) and (117), we find the lower limit for the number of needed clusters,

$$C > \max\left[40\frac{\Delta R^2}{\Delta X^2}, 10\frac{\Delta X^2}{\Delta F^2}\right]. \tag{123}$$

The first condition makes sure that enough clusters are included for slowly decaying distributions truncated smoothly with $T_{\bar{\epsilon}}(x,\bar{R})$ while the second one describes the minimum number of clusters needed to describe a narrow feature within the region of interest. If the distribution has weakly decaying tails, it is often beneficial to test different $\bar{\epsilon}$ values in the $T_{\bar{\epsilon}}(x,\bar{R})$ truncation since one can often find truncations that provide a smaller upper value C. Even when we do not know more details of the characterized distribution, the condition (123) guarantees a high level of convergence as well as an accurate mapping from the cluster expansion to the phase space. Naturally, the actual cluster expansion may converge with fewer clusters, especially when physical distributions with rapidly decaying tails are considered.

As discussed in Sec. V A, physical distributions usually have a Gaussian decay far away from their central value such that the tails of the distribution do not cause a convergence problem. Thus, the main concern is how well features within the central regions of the physical distribution can be reproduced. As a result, mostly the second condition in Eq. (123), i.e., $C>10\frac{\Delta F^2}{\Delta X^2}$, is relevant for actual distributions. This observation can immediately be transformed into a simple identification rule to qualitatively recognize which distributions may be highly correlated. From Eq. (123), we only need the quantity

$$C_{\text{phys}} \equiv 10\frac{\Delta X^2}{\Delta F^2} \tag{124}$$

to determine the level of correlations in a given distribution showing that *the ratio between the width of the narrowest feature and that of the overall distribution typically defines how correlated a physical distribution is*.

For physical probability distributions with only one peak, such as the Gaussian thermal-coherent-squeezed states, the relevant features cannot be very narrow in comparison with ΔX. As a result, such fields can always be described with relatively few clusters. Note that unphysical distributions with slowly decaying non-Gaussian tails can be single-peaked and at the same time display an appreciable $\frac{\Delta F^2}{\Delta X^2}$; see Fig. 6. Thus, they obviously need a large C for the cluster expansion to be accurate. The level of correlation increases when $P(x)$ contains multiple peaks, especially when the peaks become narrow with respect to the overall width of the distribution.

To investigate how the CET works for such highly correlated physical fields, we need to consider distributions with multiple peaks and narrow features. We already know that the Fock state $|n\rangle$ is an excellent candidate for such a highly correlated state since it has $n+1$ narrow peaks (see Fig. 7). We also consider the so-called Schrödinger-cat state [66–70],

$$|\alpha\rangle_{\text{cat}} \equiv \frac{|\alpha\rangle + |-\alpha\rangle}{\sqrt{2+2e^{-2|\alpha|^2}}}, \tag{125}$$

as another highly correlated state. If we now align the displacement along the x axis, the probability distributions in the x and y directions are

$$P(x) = \sqrt{\frac{2}{\pi}} \frac{e^{-2(x-|\alpha|)^2} + e^{-2(x+|\alpha|)^2} + 2e^{-2(x^2+|\alpha|^2)}}{2+2e^{-2|\alpha|^2}}, \tag{126}$$

$$P(y) = \sqrt{\frac{2}{\pi}} e^{-2y^2} \frac{1+\cos 4|\alpha| y}{1+e^{-2|\alpha|^2}}, \tag{127}$$

respectively. Both of these quadrature directions have multiple peaks. In the x direction, we find two separate peaks displaced by $2|\alpha|$. In the y direction, we note an interesting interference term, $1+\cos 4|\alpha|y$, whose fringe separation is also controlled by the displacement.

We next apply the CET for the Fock states $|2\rangle$ and $|4\rangle$. As discussed in Sec. V B, we anticipate that the features in the state $|2\rangle$ ($|4\rangle$) are accurately described with $C_{\text{phys}}=75$ ($C_{\text{phys}}=225$) clusters. We also investigate a Schrödinger-cat state with $\alpha=3$. In the x direction, the feature width is $\Delta F=1$ while we find width $\Delta X=3.042$. According to Eq. (124), we expect that $C_{\text{phys}}=93$ clusters are needed. The narrowest feature in the y direction now has the width $\Delta F=0.21$ while $\Delta X=\frac{1}{2}$. Together, these criteria predict that $C_{\text{phys}}=57$ clusters are needed.

The left column of Fig. 8 presents the original probability distributions (shaded area) for $|2\rangle$, $|4\rangle$, and the cat state $|\alpha\rangle_{\text{cat}}$ in the x and y directions, from top to bottom. Each frame contains also the corresponding CET with a low (blue line), medium (dashed line), and high (black circles) number of clusters included. The analysis is completed by showing the corresponding $\bar{\bar{a}}_{\Sigma,J}$ correlations in the right-hand column.

For all distributions analyzed here, the overall width is correctly reproduced even for a small C (blue lines). However, the narrow features within the region of interest are accurately described only when an elevated number of clusters is used. For all cases, the largest C (black filled squares) reproduces excellently the original distribution (shaded area). If we now look at the C_{phys} qualifiers given above, we notice that the CET indeed converges for values close to C_{phys}. This result verifies that the smallest feature size within the physical distribution determines the level of correlation of the characterized source. At the same time, we can conclude that the Fock and the Schrödinger cat states exhibit strong quantum features via strong correlations up to large cluster numbers.

As a special feature of the Schrödinger-cat state, we recognize that a correlation "packet" is formed around $\bar{\bar{a}}_{\Sigma,J}$ at

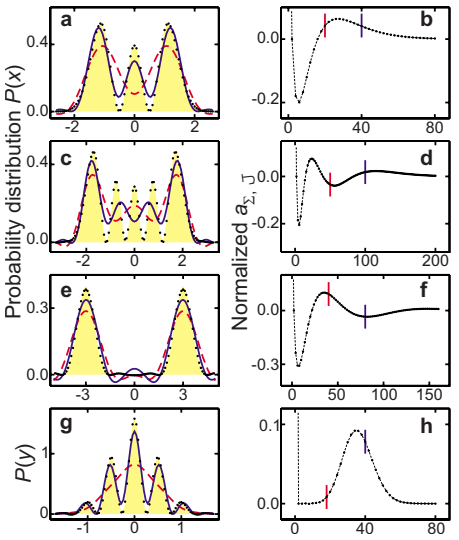

FIG. 8. (Color online) Convergence of the cluster-expansion transformation for strongly correlated physical sources. (a) The input $P(x)$ (shaded area) of Fock state $|2\rangle$ is compared with the CET result with $C=20$ (red dashed line), $C=40$ (blue line), and $C=80$ (black squares) clusters. (b) The corresponding $\bar{\bar{a}}_{\Sigma,J}$ (filled circles); the dashed line is a guide to the eye. Equivalent data are shown for (c), (d) Fock-state $|4\rangle$ as well as (e), (f) Schrödinger-cat state, with $\alpha=3$, in x- and (g), (h) y-quadrature direction.

intermediate C. However, these correlations remain relatively small even though the physical field is strongly correlated. Thus, the cluster-expansion representation not only produces a converging series of correlations, but the low-order correlations typically have more physical significance.

In Sec. V A, we have shown that physically irrelevant tails of a distribution can produce large $\bar{\bar{a}}_{\Sigma,J}$, even though the eventual CET convergence is reached with high enough C. The increase of $\bar{\bar{a}}_{\Sigma,J}$ is associated with the slowly decaying tails. Thus, it is interesting to consider how well the CET works for distributions that have no tails while they are nonanalytic; for example, $P(x)$ or its derivative could be discontinuous. We have tested the CET for several such distributions (not shown) and always find that it works excellently even in these extreme situations. As a general trend, the CET always produces a continuous distribution that approaches the discontinuous distribution as the number of clusters is increased. The mathematical convergence of the CET very much resembles how the finite Fourier transformation and its inverse reproduce a nonanalytic function as a function of the number of discrete points used in the transformation.

VI. RESTORATION OF QUANTUM-EFFICIENCY DETERIORATED DISTRIBUTIONS

As discussed in Sec. III, the marginal distribution of a light source can be directly measured using the balanced-homodyne-detection (BHD) setup [60,65]. As an experimental detail, any measurement can record an arriving photon only with an imperfect probability, $\eta<1$, that determines the quantum efficiency of the photodetectors. It is a well-established fact in quantum-state tomography that the quan-

tum efficiency of detectors η can deteriorate considerably the measured quadrature distributions $P_\eta(x)$ from their true quantum-statistical form $P(x)$ [71,72]. Vogel and Grabow formulated [71] the deterioration using

$$P_\theta^\eta(x) = \int dy g_\eta\left(y - \frac{x}{\sqrt{\eta}}\right) P_\theta^\eta(y),$$

$$g_\eta(y) = \sqrt{\frac{2}{\pi(1-\eta)}} e^{-[2\eta/(1-\eta)]y^2}, \tag{128}$$

where the original and the measured distributions are connected to the true quantum statistics via a Gaussian convolution. Since the result of a Gaussian convolution depends strongly on the integrated statistical function, the connection between measured and true quantum statistics is nontrivial when only P^η is known.

Since the measured P^η can completely mask the actual quantum features of the true P distribution, considerable research efforts have been invested to understand how the η deterioration could be removed. In particular, several papers have concluded that the restoration of the true quantum statistics from measurements is "extremely difficult" [61,72–74] when η decreases much below 1. Thus, as an alternative to measuring $P(x)$ directly with a BHD setup, several interesting suggestions and new setups have emerged to remove the η deterioration employing sequences of correlation measurements [75,76] or careful iterative optimization [77–80] of photon-statistics-resolving [81] measurements. In the following, we investigate how our cluster-expansion approach can be used to restore the true quantum-statistical distribution directly from the deteriorated P^η when η is known. In other words, we develop a scheme that allows us to use BHD measurement data to characterize the *true* quantum statistics for a wide range of η.

As shown by Herzog [82], the quantum-efficiency deterioration has a simple functional form

$$(I_K^J)_\eta \equiv \eta^{(J+K)/2} I_K^J = \eta^{(J+K)/2} \langle [\hat{B}^\dagger]^J \hat{B}^K \rangle \tag{129}$$

within the expectation-value representation. In any realistic measurement, a single photon creates a signal only with an imperfect probability defined by the quantum efficiency $\eta < 1$. Since I_K^J actually contains $(J+K)$ photon operators, the inaccuracy of the measurement attenuates it by $\eta^{(J+K)/2}$ corresponding to the total number of photon operators. Thus, we find an equally simple transformation,

$$I_{\Sigma,J}^{\eta,\theta} = \eta^{J/2} I_{\Sigma,J}^\theta, \tag{130}$$

for the collective J-photon operator.

We may now analyze what happens with the characteristics function when it is quantum statistically deteriorated. For this purpose, we insert Eq. (130) into Eq. (46), yielding

$$\chi_N^{\eta,\theta}(iq) \equiv \sum_{J=0}^{\infty} (iq)^J I_{\Sigma,J}^{\eta,\theta} = \sum_{J=0}^{\infty} (iq\sqrt{\eta})^J I_{\Sigma,J}^\theta = \chi_N^\theta(iq\sqrt{\eta}). \tag{131}$$

Consequently, the quantum-statistical deterioration can be presented via a simple rescaling of q when described via the characteristic function. Similarly, we obtain for the CER

$$\chi_N^{\eta,\theta}(iq) = e^{\xi_{\mathrm{SD}}^{\eta,\theta}(iq)} A_N^{\eta,\theta}(iq),$$

$$\xi_{\mathrm{SD}}^{\eta,\theta}(iq) = \xi_{\mathrm{SD}}^\theta(iq\sqrt{\eta}), \quad A_N^{\eta,\theta}(iq) = A_N^\theta(iq\sqrt{\eta}), \tag{132}$$

which follow by combining Eqs. (74) and (131). As a result, all relevant quantities in the cluster-expansion representation can be restored to their true quantum-statistical form by implementing

$$\xi_{\mathrm{SD}}^\theta(iq) = \xi_{\mathrm{SD}}^{\eta,\theta}\left(i\frac{q}{\sqrt{\eta}}\right), \quad A_N^\theta(iq) = A_N^{\eta,\theta}\left(i\frac{q}{\sqrt{\eta}}\right). \tag{133}$$

Thus, we have all ingredients needed to convert the deteriorated P^η into $A_N^{\eta,\theta}$ and $\xi_{\mathrm{SD}}^{\eta,\theta}$ to first restore the true A_N^θ and ξ_{SD}^θ and then the true P. More explicitly, we use the CET Eqs. (88)–(90) to produce $\xi_{\mathrm{SD}}^{\eta,\theta}$ and A_N^θ from the deteriorated input distribution $P^\eta(x)$. In the next step, we apply Eq. (133) to restore the correlated clusters. Since $A_N^\theta \xi_{\mathrm{SD}}^\theta$ are now known, we apply the steps (91) and (92) to restore the true form of the distribution function. This scheme basically defines the essential steps of the cluster expansion restoration transformation for quantum statistically deteriorated distributions.

To illustrate the CER transformation, we consider as an example how accurately the Fock-state $|2\rangle$ can be restored when the assumed measurement setup has the very low quantum efficiency, $\eta = 10\%$. By using Eqs. (49) and (128), we find the deteriorated distribution $P^\eta(x)$ (light, shaded area) shown in Fig. 9(a). In comparison with the true distribution (dark, shaded area), basically all of the characteristic features of a Fock state are washed out beyond recognition. In particular, $P^\eta(x)$ has neither nodes nor clear peaks; instead, it is a featureless distribution resembling the vacuum state more than a two-photon Fock state. Clearly, such low-quantum-efficiency data cannot be used directly for a meaningful characterization of light sources.

We proceed by constructing the $\bar{a}_{\Sigma,J}^\eta$ coefficients from $P^\eta(x)$ and then purify them following the steps explained above. The numerically generated $\bar{\bar{a}}_{\Sigma,J}^\eta$ (circles) and the restored $\bar{\bar{a}}_{\Sigma,J}$ (squares) are shown in Fig. 9(b) for the first $C = 80$ clusters. In order to check that C is large enough, we have reconstructed the input $P^\eta(x)$ from $\bar{\bar{a}}_{\Sigma,J}^\eta$; the result [filled circles in Fig. 9(a)] agrees excellently with the input distribution. Besides this, the restoration yields the $\bar{\bar{a}}_{\Sigma,J}$ format typical for the Fock state $|2\rangle$, as analyzed earlier in Fig. 8. In the last phase of CER, we use the restored correlations $\bar{\bar{a}}_{\Sigma,J}$ to convert the cluster-expasion representation back into the true distribution. The resulting $P(x)$ (squares) is shown together with the true distribution (shaded area) in Fig. 9(c). We observe that the CER produces an excellent restoration of the true quantum statistics.

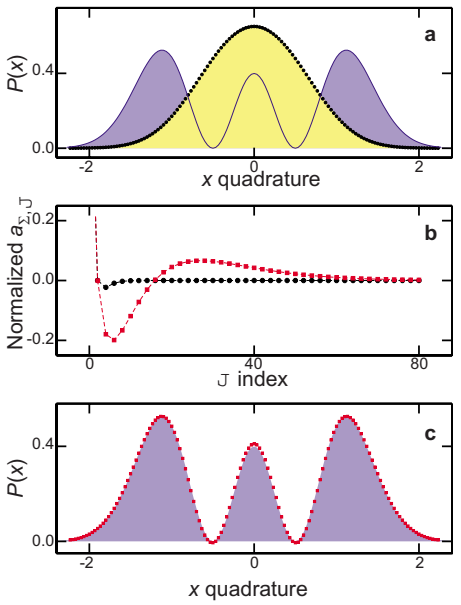

FIG. 9. (Color online) Quantum-state restoration from a quantum-statistically corrupted distribution. (a) The corrupted marginal distribution of the Fock state $|2\rangle$ after it is deteriorated by $\eta = 10\%$ is shown as the light (yellow) shaded area. The corresponding cluster-expansion transformation result is plotted as the black squares before the restoration, The true distribution is represented by the dark (blue) shaded area. (b) The corresponding deteriorated (circles) $\bar{\bar{a}}_{\Sigma,J}$ correlations are compared with the restored ones (squares). (c) The result of the cluster-expansion restoration (red squares) is compared with the true distribution (shaded area).

This example demonstrates that our CER scheme can indeed be applied to restore the true quantum statistics from corrupted measurements once the level of quantum-statistical deterioration is known. In our computation, we have discretized the input distributions into equidistant pieces separated by $\Delta x = \frac{1}{30}$. We have then applied a simple linear interpolation in evaluating the integrals (90). Thus, the solution contains the inherent numerical inaccuracy and error proportional to Δx^2. Obviously, the CER can fully overcome this numerical error since we find the true original distribution with extreme accuracy. The benefits of the CER go much beyond that; the CER can even overcome a substantial amount of experimental scatter in the input distributions to recover the true quantum statistics of the characterized source. In our future work, we will focus on exploring many of the aspects of this remarkable property.

VII. SUMMARY

We have presented how the standard quantum-optical representations of light can be defined through the concept of correlated clusters, i.e., particlelike correlations. The developed cluster-expansion transformation allows us to efficiently evaluate the one-to-one mapping between clusters and the usual phase-space and marginal distributions. In this context, our numerical examples illustrate that physical distribution can be represented through a finite number of clusters while the lower-order correlations typically dominate the properties. Especially, the manifold of coherent-, thermal-, and squeezed-state light sources can be expressed using correlations only up to two particles.

We also have performed a detailed analysis of the convergence of the cluster expansion and found two main criteria based on (i) the extension of the tails of the distribution and (ii) the width of the narrowest feature within the distribution. We observed that the cluster expansion converges rapidly when the tails decay fast enough. For slowly decaying distributions, a smooth truncation of physically irrelevant tails provides a converging cluster expansion. When the physically relevant central part of the distribution contains features that are narrow in comparison with the average width of the distribution, the analyzed source has strong correlations. As examples, we have studied Fock and Schrödinger-cat states. In both cases, the singlet-doublet correlations are still dominant even though significant correlations appear up to relatively high clusters before they eventually decay.

As the first application of the CET, we have developed the cluster-expansion restoration scheme, which allows for the retrieval of the true quantum statistics from corrupted probability distributions resulting from measurements with a low quantum efficiency. The CER can even overcome appreciable numerical inaccuracies such that it is well suited to restore quantum-tomographic measurements [60]. The fundamental reason for this remarkable property stems from CET's ability to describe the physically relevant parts of a given distribution with as few parameters as possible.

The developed CET formalism can be generalized to multimode light by following the guidelines presented in Sec. II C The found correlated clusters have a one-to-one correspondence to many-body correlations [29]. In particular, the hierarchy problem—resulting from both quantum optical and Coulombic many-body interaction—can now be solved systematically by applying the same cluster-expansion approach for quantized light and matter. We have shown what kind of correlations emerge for several relevant light fields. This information is particularly useful when quantum statistics of light is converted from light to matter, according to the principles of quantum-optical spectroscopy in semiconductors[36]. One of the major future goals will be to study how matter correlations can be controlled and characterized by the correlations imprinted to the light field.

ACKNOWLEDGMENTS

This work is supported by the Quantum Optics in Semiconductors DFG Research Group. M.K. also thanks Steven Cundiff for discussions and hospitality during his stay at JILA (University of Colorado).

APPENDIX A: SINGLET-DOUBLET FIELDS

Equation (66) introduces an ansatz for the density matrix $\hat{\rho}_{\mathrm{SD}}$ that is supposed to describe the generic singlet-doublet (SD) fields, defined by Eq. (64). We show in this appendix that the proposed $\hat{\rho}_{\mathrm{SD}}$ actually produces the singlet-doublet factorization (64). For this purpose, we start from the defini-

ton (26) to evaluate the characteristic function corresponding to $\hat{\rho}_{\mathrm{SD}}$,

$$\chi_{\mathrm{SD}}(\beta) \equiv \mathrm{Tr}[e^{\beta B^\dagger} e^{-\beta^\star B} \hat{\rho}_{\mathrm{SD}}] = \mathrm{Tr}[e^{\beta B^\dagger} e^{-\beta^\star B} D^\dagger(\alpha) S^\dagger(\gamma) \hat{\rho}_{\mathrm{th}}(N) S(\gamma) D(\alpha)], \tag{A1}$$

where the definitions (67) and (68) have been used. By applying cyclic permutations within a trace together with the basic properties of the unitary transformations S and D, we find

$$\begin{aligned}\chi_{\mathrm{SD}}(\beta) &= \mathrm{Tr}[S(\gamma)D(\alpha)e^{\beta B^\dagger} e^{-\beta^\star B} D^\dagger(\alpha) S^\dagger(\gamma) \hat{\rho}_{\mathrm{th}}(N)] \\ &= \mathrm{Tr}[e^{\beta S(\gamma)D(\alpha)B^\dagger D^\dagger(\alpha) S^\dagger(\gamma)} e^{-\beta^\star S(\gamma)D(\alpha)BD^\dagger(\alpha)S^\dagger(\gamma)} \hat{\rho}_{\mathrm{th}}(N)] \\ &= \mathrm{Tr}[e^{\beta G^\dagger} e^{-\beta^\star G} \hat{\rho}_{\mathrm{th}}(N)]. \end{aligned} \tag{A2}$$

Here, we introduce the unitary-transformed operators

$$G^\dagger \equiv S(\gamma)D(\alpha)B^\dagger D^\dagger(\alpha)S^\dagger(\gamma) = \alpha^\star + B^\dagger \cosh r - Be^{-i\phi}\sinh r,$$

$$G \equiv S(\gamma)D(\alpha)BD^\dagger(\alpha)S^\dagger(\gamma) = \alpha + B\cosh r - B^\dagger e^{i\phi}\sinh r, \tag{A3}$$

where we used the polar representation $\gamma = re^{i\phi}$ for the squeezing parameter.

To evaluate $\chi_{\mathrm{SD}}(\beta)$ further, we utilize a general operator relation

$$e^{\hat{A}}e^{\hat{B}} = e^{(1/2)[\hat{A},\hat{B}]_-} e^{\hat{A}+\hat{B}} \quad \text{if } [A,[A,B]_-]_- = [B,[A,B]_-]_- = 0, \tag{A4}$$

which simplifies Eq. (A2) into

$$\chi_{\mathrm{SD}}(\beta) = e^{(1/2)|\beta|^2 + \beta\alpha^\star - \beta^\star\alpha} \mathrm{Tr}[D(\eta)\hat{\rho}_{\mathrm{th}}(N)], \tag{A5}$$

$$\eta \equiv \beta\cosh r + \beta^\star e^{i\phi}\sinh r. \tag{A6}$$

This trace can be evaluated, leading to

$$\chi_{\mathrm{SD}}(\beta) = e^{(1/2)|\beta|^2 + \beta\alpha^\star - \beta^\star\alpha} e^{[(-1+2N)/2]|\eta|^2}. \tag{A7}$$

By inserting the definition of η, Eq. (A6), into this expression, we obtain

$$\chi_{\mathrm{SD}}(\beta) = e^{\beta\alpha^\star - \beta^\star\alpha - |\beta|^2[-(1/2)+(1/2)(1+2N)\cosh 2r]} e^{\beta^2/2[-(1/2)(1+2N)e^{-i\phi}\sinh 2r] + ([\beta^\star]^2/2)[-(1/2)(1+2N)e^{i\phi}\sinh 2r]}, \tag{A8}$$

which essentially has the same form as Eq. (64).

After these considerations, we may now determine the parameters β, ξ, and N. By comparing Eq. (64) with Eq. (A8), we can identify

$$\langle B\rangle = \beta, \tag{A9}$$

$$\Delta\langle B^\dagger B\rangle = -\frac{1}{2} + \frac{1}{2}(1+2N)\cosh 2r, \tag{A10}$$

$$\Delta\langle BB\rangle = -\frac{1}{2}(1+2N)e^{i\phi}\sinh 2r, \tag{A11}$$

where we utilized the basic properties of the hyperbolic trigonometric functions. This set of equations can be inverted yielding

$$\beta = \langle B\rangle, \tag{A12}$$

$$N = \sqrt{\left(\Delta\langle B^\dagger B\rangle + \frac{1}{2}\right)^2 - |\Delta\langle BB\rangle|^2} - \frac{1}{2}, \tag{A13}$$

$$r = \frac{1}{2}\ln\frac{\sqrt{\Delta\langle B^\dagger B\rangle + \frac{1}{2} + |\Delta\langle BB\rangle|}}{\sqrt{\Delta\langle B^\dagger B\rangle + \frac{1}{2} - |\Delta\langle BB\rangle|}}, \quad e^{i\phi} = -\frac{\Delta\langle BB\rangle}{|\Delta\langle BB\rangle|}. \tag{A14}$$

Since N must be positive for physical fields, we find the general restriction

$$|\Delta\langle BB\rangle| \leqslant \sqrt{\Delta\langle B^\dagger B\rangle(\Delta\langle B^\dagger B\rangle + 1)}. \tag{A15}$$

The identification (A12)–(A14) is rather mathematical such that we seek a more physical connection between the clusters and coherent, thermal, as well as squeezing parameters. For this purpose, we consider the Heisenberg uncertainty relation,

$$\Delta x \Delta y \geqslant \frac{1}{4}, \tag{A16}$$

where $\Delta x \equiv \sqrt{\Delta\langle\hat{x}\hat{x}\rangle} = \sqrt{\langle x^2\rangle - \langle\hat{x}\rangle\langle\hat{x}\rangle}$ (and $\Delta y \equiv \sqrt{\Delta\langle\hat{y}\hat{y}\rangle}$) is the variance fluctuation of the quadrature x (y) defined by Eq. (27). After a straightforward application of Eq. (27), we find

$$\Delta x^2 = \frac{1}{4} + \frac{1}{2}(\Delta\langle B^\dagger B\rangle + \mathrm{Re}[\Delta\langle BB\rangle]), \tag{A17}$$

$$\Delta y^2 = \frac{1}{4} + \frac{1}{2}(\Delta\langle B^\dagger B\rangle - \mathrm{Re}[\Delta\langle BB\rangle]). \tag{A18}$$

The quadrature squeezing is characterized by the maximum and minimum values

$$\Delta X \equiv \Delta x|_{\max} = \frac{1}{\sqrt{2}}\sqrt{\left(\Delta\langle B^\dagger B\rangle + \frac{1}{2}\right) + |\Delta\langle BB\rangle|}, \tag{A19}$$

$$\Delta Y \equiv \Delta y|_{\min} = \frac{1}{\sqrt{2}}\sqrt{\left(\Delta\langle B^\dagger B\rangle + \frac{1}{2}\right) - |\Delta\langle BB\rangle|}, \tag{A20}$$

respectively. With the help of these, the connections (A12)–(A14) simplify into

$$\beta = \langle B\rangle, \tag{A21}$$

$$N = 2\left(\Delta X\Delta Y - \frac{1}{4}\right), \tag{A22}$$

$$\gamma = \frac{1}{2}\frac{\Delta\langle BB\rangle}{|\Delta\langle BB\rangle|}\ln\frac{\Delta Y}{\Delta X}. \tag{A23}$$

APPENDIX B: GEOMETRIC TRANSFORMATION FROM CLUSTER-EXPANSION SEPARATION

The cluster-expansion separation (74) leads us to the Wigner function (76), which can be converted into

$$W(\alpha e^{i\phi} + \langle B\rangle) = \frac{1}{\pi^2}\int d^2\beta A_C(\beta) e^{-[(1/2)+\Delta\langle B^\dagger B\rangle - |\Delta\langle BB\rangle|]\beta_1^2 - [(1/2)+\Delta\langle B^\dagger B\rangle + |\Delta\langle BB\rangle|]\beta_2^2 e^{\beta^\star\alpha - \beta\alpha^\star}}, \tag{B1}$$

once we implement a suitable change of integration variable, $\beta \to \beta e^{i\phi}$. The phase ϕ is defined by the doublet correlation $\Delta\langle BB\rangle = |\Delta\langle BB\rangle| e^{2i\phi}$. When we identify the maximum and minimun quadrature fluctuations by using Eqs. (A19) and (A20), the Wigner function simplifies to

$$W(\alpha e^{i\phi} + \langle B\rangle) = \frac{1}{\pi^2}\int d^2\beta A_C(\beta e^{i\phi}) e^{-2\Delta Y^2\beta_1^2 - 2\Delta X^2\beta_2^2} e^{2i(\alpha_2\beta_1 - \alpha_1\beta_2)}. \tag{B2}$$

We may now introduce two new changes in integration variables $\beta_1 \to \frac{\beta_1}{2\Delta Y}$ and $\beta_2 \to \frac{\beta_2}{2\Delta X}$, to obtain

$$W(\alpha e^{i\phi} + \langle B\rangle) = \frac{1}{\pi^2 4\Delta X\Delta Y}\int d^2\beta A_C\left[\left(\frac{\beta_1}{2\Delta Y} + i\frac{\beta_2}{2\Delta X}\right)e^{i\phi}\right] e^{-(1/2)|\beta|^2} e^{2i[(\alpha_2/2\Delta Y)\beta_1 - (\alpha_1/2\Delta X)\beta_2]}. \tag{B3}$$

This result can be used to identify the scaled Wigner function and the correlation A,

$$\bar{W}(\alpha) \equiv 4\Delta X\Delta Y W([2\Delta X\alpha_1 + i2\Delta Y\alpha_2]e^{i\phi} + \langle B\rangle),$$

$$\bar{A}_C(\beta) \equiv A_C\left(\left[\frac{\beta_1}{2\Delta Y} + i\frac{\beta_2}{2\Delta X}\right]e^{i\phi}\right); \tag{B4}$$

compare Eq. (77). With these identifications, the scaled quantities are connected via

$$\bar{W}(\alpha) = \frac{1}{\pi^2}\int d^2\beta \bar{A}(\beta) e^{-(1/2)|\beta|^2} e^{-\beta^\star\alpha + \beta\alpha^\star}, \tag{B5}$$

which has the same form as Eq. (78). In particular, we have shown that the singlet-doublet separation corresponds to a simple geometric transformation (B4). A very similar derivation can be repeated for marginal distributions, eventually leading to Eqs. (85) and (86).

[1] L. Allen and J. H. Eberly, *Optical Resonance and Two-Level Atoms*, 2nd ed. (Dover, New York, 1987).
[2] D. F. Walls and G. J. Milburn, *Quantum Optics*, 1st ed. (Springer-Verlag, New York, 1994).
[3] P. Meystre and M. Sargent III, *Elements of Quantum Optics*, 3rd ed. (Springer-Verlag, New York, 1999).
[4] E. T. Jaynes and F. W. Cummings, Proc. IEEE **51**, 89 (1963).
[5] M. Tavis and F. W. Cummings, Phys. Rev. **170**, 379 (1968).
[6] B. Shore and P. L. Knight, J. Mod. Opt. **40**, 1195 (1993).
[7] G. Lindblad, Commun. Math. Phys. **48**, 119 (1976).
[8] J. Dalibard, Y. Castin, and K. Mølmer, Phys. Rev. Lett. **68**, 580 (1992).
[9] H. J. Carmichael, Phys. Rev. Lett. **70**, 2273 (1993).
[10] Y. Kaluzny, P. Goy, M. Gross, J. M. Raimond, and S. Haroche, Phys. Rev. Lett. **51**, 1175 (1983).
[11] R. J. Thompson, G. Rempe, and H. J. Kimble, Phys. Rev. Lett. **68**, 1132 (1992).
[12] M. Brune, F. Schmidt-Kaler, A. Maali, J. Dreyer, E. Hagley, J. M. Raimond, and S. Haroche, Phys. Rev. Lett. **76**, 1800 (1996).
[13] P. G. Kwiat, K. Mattle, H. Weinfurter, A. Zeilinger, A. V. Sergienko, and Y. Shih, Phys. Rev. Lett. **75**, 4337 (1995).
[14] J. Raimond, M. Brune, and S. Haroche, Rev. Mod. Phys. **73**, 565 (2001).
[15] P. Shor, *Algorithms for Quantum Computation: Discrete Logarithms and Factoring*, in *Proceedings of the 35th Annual Symposium on the Foundations of Computer Science*, edited by S. Goldwasser (IEEE Computer Society, Los Alamitos, CA, 1994), p. 124.
[16] A. Ekert and R. Jozsa, Rev. Mod. Phys. **68**, 733 (1996).
[17] D. Bouwmeester, J.-W. Pan, K. Mattle, M. Eibl, H. Weinfurter, and A. Zeilinger, Nature **390**, 575 (1997).
[18] A. Furusawa, J. Sørensen, S. Braunstein, C. Fuchs, H. Kimble, and E. Polzik, Science **282**, 706 (1998).
[19] M. Riebe, H. Häffner, C. Roos, W. Hänsel, J. Benhelm, G. Lancaster, T. Körber, C. Becher, F. Schmidt-Kaler, D. James, and R. Blatt, Nature **429**, 734 (2004).
[20] M. Barrett, J. Chiaverini, T. Schaetz, J. Britton, W. Itano, J. Jost, E. Knill, C. Langer, D. Leibfried, R. Ozeri, and D. Wineland, Nature **429**, 737 (2004).
[21] R. Glauber, Phys. Rev. **131**, 2766 (1963).
[22] E. Sudarshan, Phys. Rev. Lett. **10**, 277 (1963).
[23] M. Hillery, R. O'Connel, M. Scully, and E. Wigner, Phys. Rep. **106**, 121 (1984).
[24] R. E. Slusher, L. W. Hollberg, B. Yurke, J. C. Mertz, and J. F. Valley, Phys. Rev. Lett. **55**, 2409 (1985).
[25] H. J. Kimble, M. Dagenais, and L. Mandel, Phys. Rev. Lett. **39**, 691 (1977).
[26] P. Michler, A. Kiraz, C. Becher, W. V. Schoenfeld, P. M. Petroff, L. D. Zhang, E. Hu, and A. Imamoglu, Science **290**, 2282 (2000).
[27] A. I. Lvovsky, H. Hansen, T. Aichele, O. Benson, J. Mlynek, and S. Schiller, Phys. Rev. Lett. **87**, 050402 (2001).
[28] W. Tittel, J. Brendel, H. Zbinden, and N. Gisin, Phys. Rev. Lett. **81**, 3563 (1998).
[29] M. Kira and S. W. Koch, Prog. Quantum Electron. **30**, 155 (2006).
[30] M. Kira, F. Jahnke, S. W. Koch, J. D. Berger, D. V. Wick, T. R. Nelson, Jr., G. Khitrova, and H. M. Gibbs, Phys. Rev. Lett. **79**, 5170 (1997).
[31] M. Kira, F. Jahnke, and S. W. Koch, Phys. Rev. Lett. **81**, 3263 (1998).
[32] M. Kira, F. Jahnke, and S. W. Koch, Phys. Rev. Lett. **82**, 3544 (1999).
[33] Y.-S. Lee, T. B. Norris, M. Kira, F. Jahnke, S. W. Koch, G. Khitrova, and H. M. Gibbs, Phys. Rev. Lett. **83**, 5338 (1999).
[34] C. Ell, P. Brick, M. Hübner, E. S. Lee, O. Lyngnes, J. P. Prineas, G. Khitrova, H. M. Gibbs, M. Kira, F. Jahnke, S. W. Koch, D. G. Deppe, and D. L. Huffaker, Phys. Rev. Lett. **85**, 5392 (2000).
[35] W. Hoyer, M. Kira, S. W. Koch, H. Stolz, S. Mosor, J. Sweet, C. Ell, G. Khitrova, and H. M. Gibbs, Phys. Rev. Lett. **93**, 067401 (2004).
[36] M. Kira and S. W. Koch, Phys. Rev. A **73**, 013813 (2006).
[37] V. V. Kocharovsky, V. V. Kocharovsky, and M. O. Scully, Phys. Rev. Lett. **84**, 2306 (2000).
[38] C. Cohen-Tannoudji, J. Dupont-Roc, and G. Grynberg, *Photons & Atoms*, 3rd ed. (Wiley, New York, 1989).
[39] M. Kira, F. Jahnke, W. Hoyer, and S. W. Koch, Prog. Quantum Electron. **23**, 189 (1999).
[40] H. Haug and S. W. Koch, *Quantum Theory of the Optical and Electronic Properties of Semiconductors*, 4th ed. (World Scientific, Singapore, 2004).
[41] K. Brueckner, Phys. Rev. **100**, 36 (1955).
[42] H. W. Wyld and B. D. Fried, Ann. Phys. (N.Y.) **23**, 374 (1963).
[43] J. Cízek, J. Chem. Phys. **45**, 4256 (1966).
[44] G. D. Purvis and R. J. Bartlett, J. Chem. Phys. **76**, 1910 (1982).
[45] F. E. Harris, H. J. Monkhorst, and D. L. Freeman, *Algebraic and Diagrammatic Methods in Many-Fermion Theory*, 1st ed. (Oxford Press, New York, 1992).
[46] J. Fricke, Ann. Phys. (N.Y.) **252**, 479 (1996).
[47] M. Kira, W. Hoyer, T. Stroucken, and S. W. Koch, Phys. Rev. Lett. **87**, 176401 (2001).
[48] S. W. Koch, M. Kira, G. Khitrova, and H. M. Gibbs, Nat. Mater. **5**, 523 (2006).
[49] M. Kira and S. W. Koch, Eur. Phys. J. D **36**, 143 (2005).
[50] M. Kira, W. Hoyer, and S. W. Koch, Solid State Commun. **129**, 733 (2004).
[51] M. Kira and S. W. Koch, Phys. Rev. Lett. **93**, 076402 (2004).
[52] M. Kira, W. Hoyer, S. W. Koch, P. Brick, C. Ell, M. Hübner, G. Khitrova, and H. M. Gibbs, Semicond. Sci. Technol. **18**, S405 (2003).
[53] K. J. Ahn, J. Förstner, and A. Knorr, Phys. Rev. B **71**, 153309 (2005).
[54] N. Baer, C. Gies, J. Wiersig, and F. Jahnke, Eur. Phys. J. B **50**, 411 (2006).
[55] M. Richter, T. Renger, G. Renger, and A. Knorr, J. Chem. Phys. **127**, 075105 (2007).
[56] T. Thiele, *Theory of Observations*, 1st ed. (Charles & Edwin Layton, London, 1903).
[57] R. Fisher and J. Wishart, Proc. London Math. Soc. **33**, 195 (1932).
[58] H. P. Yuen and J. H. Shapiro, IEEE Trans. Inf. Theory **26**, 78 (1980).
[59] H. P. Yuen and V. W. S. Chan, Opt. Lett. **8**, 177 (1983).
[60] D. T. Smithey, M. Beck, M. G. Raymer, and A. Faridani, Phys. Rev. Lett. **70**, 1244 (1993).
[61] M. G. Raymer, J. Cooper, and H. Carmichael, J. Opt. Soc. Am.

B **12**, 1801 (1993).
[62] P. Kelley and W. Kleiner, Phys. Rev. **136**, A316 (1964).
[63] R. Glauber, in *Quantum optics and electronics*, edited by C. de Witt, C. Blandin, and C. C. Tannoudji, Gordon and Breach, New York, 1965.
[64] E. Wigner, Phys. Rev. **40**, 749 (1932).
[65] K. Vogel and H. Risken, Phys. Rev. A **40**, 2847 (1989).
[66] B. Yurke and D. Stoler, Phys. Rev. Lett. **57**, 13 (1986).
[67] M. Brune, S. Haroche, J. Raimond, L. Davidovich, and N. Zagury, Phys. Rev. A **45**, 5193 (1992).
[68] M. Dakna, T. Anhut, T. Opatrny, L. Knöll, and D.-G. Welsch, Phys. Rev. A **55**, 3184 (1997).
[69] T. Azim, S. Qamar, and M. Zubairy, J. Mod. Opt. **49**, 245 (2002).
[70] A. Ourjoumtsev, R. Tualle-Brouri, J. Laurat, and P. Grangier, Science **312**, 83 (2006).
[71] W. Vogel and J. Grabow, Phys. Rev. A **47**, 4227 (1993).
[72] U. Leonhardt and H. Paul, Phys. Rev. A **48**, 4598 (1993).
[73] T. Kiss, U. Herzog, and U. Leonhardt, Phys. Rev. A **52**, 2433 (1995).
[74] T. Kiss, U. Herzog, and U. Leonhardt, Phys. Rev. A **57**, 3134 (1998).
[75] H. Paul, P. Törma, T. Kiss, and I. Jex, Phys. Rev. Lett. **76**, 2464 (1996).
[76] E. Shchukin and W. Vogel, Phys. Rev. Lett. **96**, 200403 (2006).
[77] A. R. Rossi, S. Olivares, and M. G. A. Paris, Phys. Rev. A **70**, 055801 (2004).
[78] G. Zambra, A. Andreoni, M. Bondani, M. Gramegna, M. Genovese, G. Brida, A. Rossi, and M. G. A. Paris, Phys. Rev. Lett. **95**, 063602 (2005).
[79] Z. Hradil, D. Mogilevtsev, and J. Rehácek, Phys. Rev. Lett. **96**, 230401 (2006).
[80] D. Achilles, C. Silberhorn, and I. A. Walmsley, Phys. Rev. Lett. **97**, 043602 (2006).
[81] K. Banaszek and K. Wodkiewicz, Phys. Rev. Lett. **76**, 4344 (1996).
[82] U. Herzog, Phys. Rev. A **53**, 1245 (1996).